NASA Contractor Report 181838

Transient Hot-Film Sensor Response in a Shock Tube

A.S. Roberts, Jr., K.R. Ortgies, and E. Gartenberg

Old Dominion University Research Foundation
Norfolk, Virginia 23529

Contract NAG1-735
May 1989

National Aeronautics and
Space Administration

Langley Research Center
Hampton, Virginia 23665

ABSTRACT

Shock tube experiments have been performed to determine the response of a hot-film sensor, mounted flush on the side-wall of a shock tube, to unsteady flow behind a normal shock wave. The present experiments attempt to isolate the response of the anemometer due only to the change in convective heat transfer at the hot-film surface. The experiments, performed at low supersonic shock speeds in air, are described along with the data acquisition procedure. The change in convective heat transfer is deduced from the data and the results are compared with those from transient boundary-layer theory and another set of experimental results. Finally, a transient local heat transfer coefficient is formulated for use as the forcing function in a hot-film sensor instrument model simulation.

TABLE OF CONTENTS

LIST OF TABLES

LIST OF FIGURES

LIST OF SYMBOLS

A	sensor surface area, 1.97×10^{-3} cm^2
c_f	local skin friction coefficient
c_p	specific heat at constant pressure, kJ/kg·K
Ec	Eckert number, $\frac{\bar{u}_e^2}{c_{p,w}(T_w - T_e)}$
$f(\eta)$	function defined by Eq. (2.7)
h	local heat transfer coefficient, $W/m^2 \cdot K$
I	bridge current, A
k	thermal conductivity, W/m·K
Nu	local Nusselt number, $\frac{hx}{k}$
P	electrical power, W
P_1	undisturbed gas pressure
P_2	driven shocked gas pressure
P_4	driver gas pressure
q	rate of heat transfer in +y-direction, W
q''	heat flux in +y-direction, W/m^2
R	Universal gas constant
Rc	cable resistance, 1.77 Ω
Rs	hot-film sensor resistance, Ω
Re	Reynolds number
$r(\eta)$	function defined by Eq. (2.10)
$s(\eta)$	function defined by Eq. (2.12)

St	local Stanton number
T	absolute static temperature, K
T_m	mean reference temperature defined by Eq. (2.25)
T_r	recovery temperature, K
t	time, s
u,v	velocities parallel to x,y-axes, m/s
u_w	velocity of wall in x,y-coordinate system, m/s
$\bar{u},\bar{v}$	velocities parallel to $\bar{x},\bar{y}$-axes, m/s
V	voltage, V
x,y	coordinates stationary with respect to wave
$\bar{x},\bar{y}$	coordinates stationary with respect to wall
η	similarity parameter, Eq. (2.6)
μ	coefficient of viscosity, Pa·s
ν	kinematic viscosity, m^2/s
ρ	mass density, kg/m^3
σ	Prandtl number, $\mu c_p/k$
τ_w	local shear stress exerted by fluid on wall
ϵ	initial transient response time
Δ	incremental change
θ	momentum boundary-layer thickness
$\tilde{\delta}$	velocity boundary-layer thickness

Subscripts:

b	undisturbed flow ahead of wave
e	flow external to fluid boundary layer

m	quantity evaluated at T_m
w	quantity evaluated just above wall surface or at wall temperature
s	sensor
B	total bridge output
amb	ambient conditions
ref	reference power level
conv	convective heat transfer
xp	fluid particle behind shock wave
xs	shock wave fluid particle

Superscripts:

$'$	denotes differentiation with respect to η
*	derived with respect to T_e

CHAPTER 1
INTRODUCTION

The transient response of a constant temperature hot-film sensor, mounted on the side wall of a shock tube, due to the passage of a moving normal shock wave and the ensuing convective heat transfer is analyzed. Also included is an interpretation of transient, compressible boundary-layer theory for application to shock tube experiments with heat convected from a side wall mounted hot-film sensor. This type of sensor is currently in use by many researchers doing experimental wind tunnel research. The effective use of this sensor requires a knowledge of its steady-state, as well as its transient response characteristics due to changes in flowfield conditions. The experimental steady-state response characteristics have been documented by Wusk, et al [1]*. To obtain the transient response characteristics, a shock tube is used to induce an unsteady, compressible boundary-layer flow across the hot-film sensor.

---

*Numbers in brackets refer to the list of references.

1.1 Motivation

Hot-film sensors are currently being used experimentally for many purposes, including the detection of transition from laminar to turbulent flow in a flowfield [2]. The research presented in this thesis was originally motivated by a desire to use a hot-film anemometer in the detection and measurement of cross-flow vortices [1]. In order to solve this problem, an understanding of the transient response characteristics of the hot-film sensor must be known. Consequently, this work is limited to analyzing the transient response of the hot-film sensor due to an almost instantaneous step-change in convective flow conditions. Furthermore, the research is directed by the desire to correlate the experimental results with existing transient boundary-layer theory [3]. This work will be of interest to those using hot-film sensors for various applications, because a knowledge of the sensor's steady and transient response assures a more accurate means of characterizing flow over a surface.

1.2 General Problem Description

The general problem treated in this thesis is to analyze the transient response of a constant-temperature hot-film sensor from shock tube experiments in order to determine how the convective heat transfer varies with time, and correlate these results with existing transient boundary-layer theory. Consequently, the hot-film sensor

response can then be predicted under variable flow conditions.

Normal shock theory indicates that a step change in pressure, temperature, and velocity occurs across the wave. A sudden change in flow properties causes a transient response in the hot-film sensor. Because the normal shock wave is moving in the laboratory frame of reference, a transient boundary layer develops, and the hot-film sensor responds to the change in convective heat transfer occurring at the sensor with a change in the anemometer output voltage. The subsequent boundary-layer build-up after the passage of the initial normal shock wave indicates that the boundary-layer thickness increases, which in turn decreases the convective transport of energy from the sensor as time increases. Theoretical work in the determination of the compressible boundary layer behind a moving normal shock has been done by Mirels [3,4].

1.3 Relevant Literature

The development of the theoretical prediction of the transient convective heat transfer behind a moving normal shock was accomplished in two papers published by Mirels [3,4]. The first paper predicts the laminar velocity boundary-layer characteristics as well as the thermal boundary-layer characteristics behind a moving normal shock advancing into a stationary fluid [4]. The second of these two papers predicts the thermal and velocity boundary layer

profiles for both laminar and turbulent flow behind a shock or thin expansion wave advancing into a stationary fluid [3]. These works are used extensively in this thesis as the basis for predicting the theoretical velocity and thermal boundary layer profiles across the hot-film sensor. DISA, a Denmark manufacturer of thermal anemometry instrumentation, produced results for hot-wire anemometers which qualitatively corroborate with the anemometer response for the shock tube tests done in this thesis research [5]. Wusk, Carraway, and Holmes use an arrayed hot-film sensor for laminar boundary-layer studies aimed toward the detection of cross-flow vortices [1]. Furthermore, the same type of constant temperature hot-film sensor, which is employed in the present research, was tested by Wusk, et al. The arrayed hot-film sensor was mounted on a NASA NLF(1)-0414 natural laminar flow airfoil and tested in the NASA Langley Instrument Research Division (IRD) small calibration facility. The goal of that research was to take the initial steps in the steady-state calibration of the hot-film sensor under constant flow conditions for the detection of spanwise variations of heat transfer. In the DISA work, a hot-wire anemometer was moved radially from the shock tube axis to within 0.05 mm of the wall of the shock tube to measure the shock front curvature. Also, a comparison of the experimental results from this thesis is made with the work by Davies and Bernstein [6]. In the experimental investigation by

Davies and Bernstein, a semi-infinite flat plate was mounted in the low-pressure chamber of a shock tube in order to determine the convective heat transfer rate due to a shock-induced boundary layer. Furthermore, Davies and Bernstein also use Mirels' works [3,4] for correlation with their experimental measurements.

A paper published by Roberts, et al [13] used high frequency response (typically of order 10^6 Hz) miniature surface thermocouples mounted on the surface of the Austrailian National University (ANU) T3 shock tube to detect convective heat transfer and compare the heat transfer on "clean" and "dusty" surfaces. The research had test times on the order of 200 μs due to the very high pressures at which the tests were conducted. Roberts, et al illustrates a comparison of his results with that of Mirels' turbulent boundary-layer theory [3].

1.4 Problem Statement

The problem to be analyzed in this thesis is the variation of convective heat transfer with time due to thermal and velocity boundary-layer growth behind a moving normal shock wave across a constant-temperature hot-film sensor. A shock tube is used as the experimental means of analyzing this problem. As the shock passes over the sensor, a flow is induced behind the normal shock wave which causes the convective heat transfer above the hot-film sensor to change, and thus produces a change in the

anemometer output voltage. The purpose of this thesis is to measure the transient convective heat transfer using the surface temperature and heat transfer rate provided by the hot-film sensor. Results are compared with experimental results of other researchers, and correlated with transient, compressible boundary-layer theory.

In the following chapter, the transient, compressible boundary-layer theory is presented and briefly discussed. The theoretical formulations applied in this thesis are interpretations taken from Mirels' works [3,4] regarding the prediction of the boundary-layer growth behind a moving normal shock wave. The following chapter contains the reference frame transformation used to modify the governing equations into a more useful form. Also presented are the laminar and turbulent correlations for the convective heat transfer.

CHAPTER 2
THEORETICAL FORMULATIONS

2.1 Reference Frame Transformations

A boundary layer is established along the shock tube wall and across the hot-film sensor as the normal shock wave passes. The boundary-layer growth affects the convective heat transfer rate from the sensor. The normal shock wave is assumed to travel at a constant velocity, parallel to the wall, into a stationary fluid. The choice of coordinate systems for the theoretical analysis is considered here in some detail.

A coordinate system, $\bar{x}$ and $\bar{y}$, is fixed with respect to the shock tube wall. The corresponding velocities are $\bar{u}$, $\bar{v}$. In this coordinate system, the wave is moving at a constant velocity and is considered to move in a time dependent (i.e. unsteady) reference frame. In order to make simplifications in the governing equations, the application of a steady reference frame is required. A coordinate system is employed in which the wave is considered stationary and the wall is moving at a constant velocity equal in magnitude to the shock wave velocity in the unsteady reference frame. In this reference frame, x and y represent the coordinates fixed to and moving with

the wave. The corresponding velocities in this reference frame are u and v. By selecting this reference frame, the coordinate system is moving with the constant wave velocity and the flow is considered steady. Figure 2.1 illustrates the coordinate systems used in the theoretical analysis.

The following assumptions are employed in order to develop the governing equations in a more useful form. Because the coordinate system is moving with the wave, the time derivative terms in the governing equations are zero. With laminar boundary-layer flow, retaining compressibility effects and assuming dP/dx=0, the Prandtl boundary-layer equations apply for flow near the wall [7]. By assuming the wave to travel at a constant velocity, the velocity of the flow behind the wave is also traveling at a constant velocity. Because of this assumption and the fact that the sensor is treated as a flat plate, Bernoulli's equation is employed to validate the assumption dP/dx=0. Consequently, the governing equations are:

Continuity,

$$\frac{\partial(\rho u)}{\partial x} + \frac{\partial(\rho v)}{\partial y} = 0 \qquad (2.1)$$

Momentum,

$$u\frac{\partial u}{\partial x} + v\frac{\partial u}{\partial y} = \frac{1}{\rho}\frac{\partial}{\partial y}\left[\mu\frac{\partial u}{\partial y}\right] \qquad (2.2)$$

Energy,

$$\rho c_p\left[u\frac{\partial T}{\partial x} + v\frac{\partial T}{\partial y}\right] = \frac{\partial}{\partial y}\left[k\frac{\partial T}{\partial y}\right] + \mu\left[\frac{\partial u}{\partial y}\right]^2 \qquad (2.3)$$

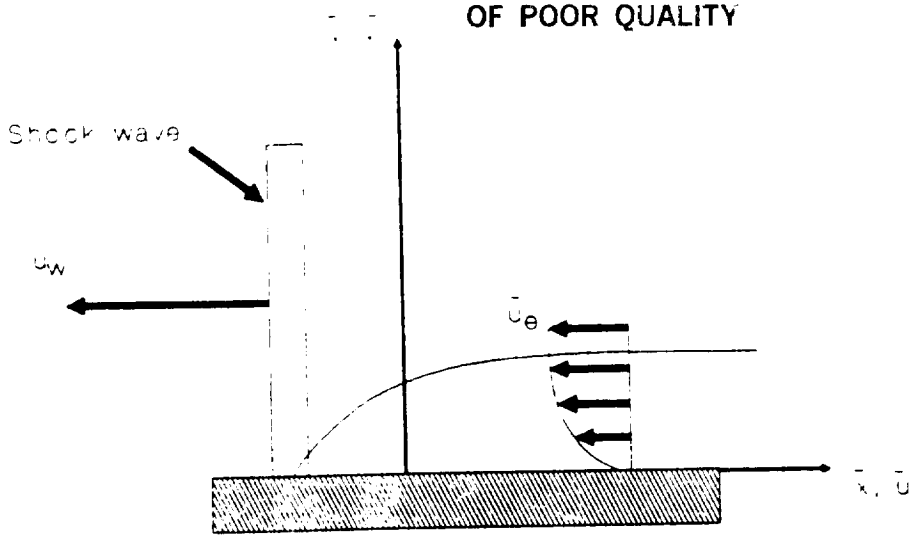

(a) With respect to lab

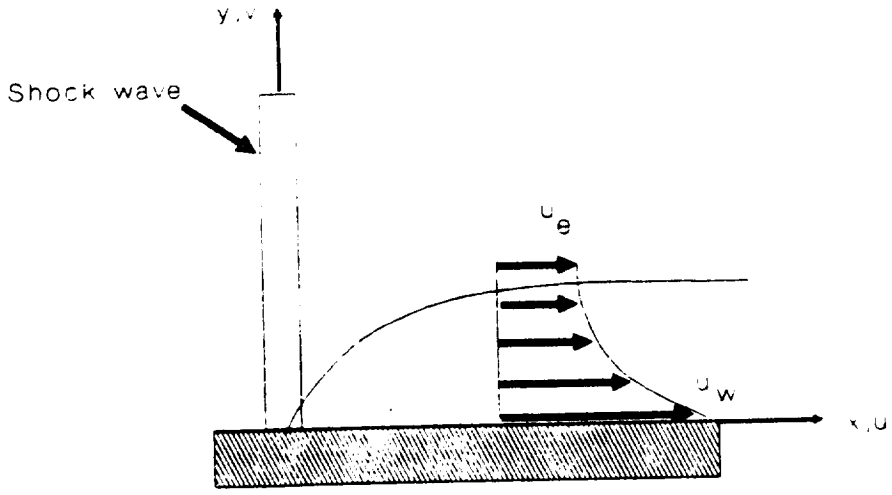

(b) With respect to wave

Figure 2.1. Coordinate Systems Used in Theoretical Boundary Layer Analysis

Ideal Gas Law,

$$P = \rho RT = \text{const.} \tag{2.4}$$

subject to: $(x > 0)$

$$\begin{aligned} u(x,0) &= u_w \qquad u(x,\infty) = u_e \\ v(x,0) &= 0 \\ T(x,0) &= T_w \qquad T(x,\infty) = T_e \end{aligned} \tag{2.5}$$

2.2 Similarity Transformation of Governing Equations

The governing equations can be transformed to a form that is easily integrated numerically. From Mirels [3], variable transport and thermal properties are applied in which μ and k are assumed proportional to T. Also, c_p and σ are assumed to be independent of T, but are evaluated at the wall temperature, T_w. The thermal and transport properties are arbitrarily referenced to the wall. Defining the similarity parameter as:

$$\eta = \sqrt{\frac{u_e}{2x\nu_w}} \int_0^y \frac{T_w}{T(x,y)}\, dy \tag{2.6}$$

the governing equations can be transformed by the usual boundary layer similarity transformations. Thus, the non-linear momentum equation becomes:

$$f''' + ff'' = 0 \tag{2.7}$$

subject to:

$$\begin{aligned} f(0) &= 0 \\ f'(0) &= \frac{u_w}{u_e} \\ f'(\infty) &= 1 \end{aligned} \tag{2.8}$$

The transformed energy equation is linear and can be expressed as a linear superposition of the solutions for the case with zero heat transfer plus the case with heat transfer [3]. Consequently, the energy equation becomes:

$$\frac{T}{T_e} = 1 + \left[\frac{u_w}{u_e}-1\right]^2 \frac{u_e^2\, r(\eta)}{2T_e c_{p,w}} + \left[\frac{T_w}{T_e} - \frac{T_r}{T_e}\right] s(\eta) \qquad (2.9)$$

where the functions $r(\eta)$ and $s(\eta)$ are determined as follows:

Zero Heat Transfer Case,

$$r'' + \sigma_w f r' = \frac{-2\sigma_w}{\left[\frac{u_w}{u_e}-1\right]^2} (f'')^2 \qquad (2.10)$$

subject to:

$$r(\infty) = r'(0) = 0 \qquad (2.11)$$

and Heat Transfer Case,

$$s'' + \sigma_w f s' = 0 \qquad (2.12)$$

subject to:

$$s(0) = 1 \qquad (2.13)$$

$$s(\infty) = 0$$

High speed convective heat transfer is accomplished with respect to a recovery temperature, T_r, which takes the form:

$$\frac{T_r}{T_e} = 1 + \left[\frac{u_w}{u_e}-1\right]^2 \frac{u_e^2 r(0)}{2T_e c_{p,w}} \qquad (2.14)$$

With the energy equation defined by equation (2.9), a further reduction may be expressed in terms of the convective heat flux at the shock tube wall:

$$q''_w = \left[-k\frac{\partial T}{\partial y}\right]_w = -k_w s'(0)\sqrt{\frac{u_e}{2x\nu_w}}\,(T_w - T_r) \qquad (2.15)$$

This equation becomes the most useful form in comparing the experimental data to the theory for laminar flow conditions.

2.3 Laminar Correlation

The laminar correlation for the convective heat transfer occurring above the hot-film sensor is developed from the governing equations using the similarity and reference frame transformations. Because radiative and conductive heat transfer effects are neglected, the resulting equation for the heat transfer from the hot-film sensor is that of convective heat transfer. By definition, the convective heat flux in high velocity boundary-layer flow is defined:

$$q'' = h(T_w - T_r) \qquad (2.16)$$

A direct substitution with Eq. (2.15) results in an expression for the convective heat transfer coefficient, h. Due to the reference frame transformation, Eq. (2.15) is valid for a coordinate system moving with the shock wave velocity. Since the experimental results are gathered in the laboratory (i.e. unsteady) frame of reference, the theoretical equations are transformed to the lab reference frame to maintain consistency between theoretical and experimental results. Consequently, the equations are

initially derived in the wave reference frame and transformed to the lab reference frame by initiating the following substitutions for position and velocity, respectively:

$$\bar{x} = u_w t - x \tag{2.17}$$

$$\bar{u}_e = u_w - u_e \tag{2.18}$$

By utilizing these relations, the convective heat transfer coefficient becomes:

$$h = \frac{-k_w s'(0)}{\sqrt{2\nu_w t}} \tag{2.19}$$

The convective heat transfer coefficient becomes a function only of time, t.

As stated in Section 1.4, an objective of this thesis is to compare the results of this thesis to the work of Davies and Bernstein [6]. In order to make this comparison, the Reynolds, Nusselt, and Stanton numbers are defined. Mirels [3] defines a Reynolds number with respect to a fluid particle traveling behind an expansion wave in a stationary (lab) reference frame. Applying Mirels' definition of Reynolds number to a shock wave and employing Eqs. (2.17) and (2.18), a local Reynolds number for the fluid particle behind the wave in the lab frame of reference is defined:

$$Re_{xp} = \frac{(u_w - u_e)^2 t}{\nu_w} \tag{2.20}$$

Davies and Bernstein [6] illustrate their results using a

Reynolds number defined with respect to a fluid particle traveling with the shock velocity. The following substitution transforms Eq. (2.20) into a Reynolds number defined with respect to a fluid particle traveling with the shock velocity:

$$Re_{xs} = Re_{xp}\left[\frac{u_w}{u_e}\right] \tag{2.21}$$

The Nusselt number is a non-dimensional temperature gradient, when surface and free stream temperatures are fixed, and provides a measure of the convective heat transfer occurring at the surface. Since a change in reference frame is used to transform the governing equations into steady boundary-layer equations, the Nusselt and Stanton numbers are therefore defined in this steady reference frame and then transformed into the laboratory (unsteady) reference frame. By definition, the Nusselt number, with respect to the shock wave reference frame, is defined as:

$$Nu = \frac{hx}{k_w} \tag{2.22}$$

After substituting Eqs. (2.17) and (2.19) into Eq. (2.22), the Nusselt number takes the form:

$$Nu = \frac{-s'(0)\sqrt{Re_{xp}}}{\sqrt{2}\left[\frac{u_w}{u_e}-1\right]} \tag{2.23}$$

As an alternative to using the Nusselt number for the dimensionless convective heat transfer parameter, the Stanton number (modified Nusselt number) is used. The

derived Stanton number takes the form:

$$St = \frac{-s'(0)}{\sigma_w \sqrt{2\left[\frac{u_w}{u_e}-1\right]}\sqrt{Re_{xp}}} \qquad (2.24)$$

This equation is then applied to compare this work with the work of Davies and Bernstein [6]. These derivations are necessary for laminar flow conditions; however, Mirels [3] develops a turbulent correlation that is presented in the following section.

2.4 Turbulent Correlation

The turbulent boundary-layer solution for convective heat transfer behind a moving expansion wave has been developed in detail by Mirels [3]. The solution is obtained for a moving shock wave by extending empirical, semi-infinite flat plate boundary-layer theory to the case of a moving wall. Mirels [3] assumes a $(1/7)^{th}$ power velocity profile and extends this profile to a moving wall. Also, compressible turbulent flow over a semi-infinite flat plate is approximated by evaluating the fluid properties at a mean static temperature, T_m, for the Blasius relation of incompressible turbulent flow past a semi-infinite flat plate [3]. A reasonable estimate for the mean temperature, T_m is given by Eckert [11]:

$$T_m = 0.5(T_w+T_e) + 0.22(T_r-T_e) \qquad (2.25)$$

The final expression of the integral form of the momentum equation, after appling the Blasius relation, takes the

form:

$$\frac{\tau_w}{\rho_e u_e^2} = 0.0460\cdot(\theta/\tilde{\delta})\left[\frac{\varphi\left[\frac{u_w}{u_e}-1\right]}{(\theta/\tilde{\delta})}\right]^{\frac{4}{5}}\left|\frac{u_w}{u_e}-1\right|^{\frac{3}{5}}\left[\frac{\nu_e}{u_e x}\right]^{\frac{1}{5}} \qquad (2.26)$$

where,

$$\varphi = \left[\frac{\mu_m}{\mu_e}\right]^{\frac{1}{4}}\left[\frac{T_e}{T_m}\right]^{\frac{3}{4}} \qquad (2.27)$$

and $(\theta/\tilde{\delta})$ is the ratio of the boundary-layer momentum thickness to the fluid velocity boundary-layer thickness [3, defined by Eq.(46a)].

The Reynolds-Colburn analogy [12]:

$$St\sigma^{\frac{2}{3}} = \frac{c_f}{2} \qquad (2.28)$$

is applied with the skin friction coefficient defined with respect to the lab reference frame as:

$$c_f = \frac{\tau_w}{\frac{1}{2}\rho_w[u_w-u_e]^2} \qquad (2.29)$$

and substituting Eqs. (2.26), (2.28) and (2.29), the final equation for the convective heat transfer behind a moving normal shock in a compressible, turbulent, boundary-layer flow takes the form:

$$St\cdot Re_{xp}^{\frac{1}{5}} = 0.0460\cdot\left[\frac{T_w}{T_e}\,\frac{\theta}{\tilde{\delta}}\,\frac{1}{\left[1-\frac{u_w}{u_e}\right]}\right]^{\frac{1}{5}}\sigma_m^{-\frac{2}{3}} \qquad (2.30)$$

Thus, a comparison of the theory for a compressible, unsteady, turbulent-boundary layer flow can be made with the work by Davies and Bernstein [6] as well as Roberts, et al [13], and with experimental results developed here.

From the definition of Stanton number:

$$St = \frac{Nu}{\sigma Re_{xp}} \tag{2.31}$$

and applying Eqs. (2.20), (2.22), and (2.30), a turbulent heat transfer coefficient is derived. Furthermore, Mirels [3] neglects the variation of fluid state properties which results in a simplification of Eq. (2.30). The turbulent convective heat transfer coefficient takes the form:

$$h = \frac{0.0460 \cdot k_m \sigma_m^{\frac{1}{3}} (u_w - u_e)^{\frac{3}{5}} \left[\frac{T_w}{T_e} \frac{\theta}{\delta} \left[\frac{1}{1 - \frac{u_w}{u_e}} \right] \right]^{\frac{1}{5}}}{\nu_m^{\frac{4}{5}} t^{\frac{1}{5}}} \tag{2.32}$$

The experimental procedures and set-up for the shock tube tests conducted using the NASA Langley Shock Tube are discussed in the following chapter. Also presented are the equations used to reduce the experimental data into a form for comparison with the theoretical results and with experimental work done by Davies and Bernstein [6] and Roberts, et al [13].

CHAPTER 3
SHOCK TUBE EXPERIMENT

3.1 Purpose

The shock tube is utilized as the test apparatus for the analysis of the transient response of a hot-film sensor on a foam substrate mounted flush in the shock tube wall. The shock tube is utilized as the test apparatus because an almost instantaneous step-change in flow properties is obtained across the moving normal shock as the shock passes over the sensor, and thereby causes a transient boundary-layer build-up. Also, the unconstrained access and simplicity in operating the shock tube cannot be overlooked as a driving force in the decision to utilize the shock tube as the test apparatus for transient response experiments. The ultimate goal behind the experiment is to determine the hot-film anemometer response due to variations in convective flow conditions and to ascertain the repeatability of the experimental results.

3.2 Experimental Set-up

The equipment utilized in the test is listed in Appendix A. The actual shock tube assembly used for the tests is seen in Fig. 3.1. The experimental equipment configuration outlining the flow of experimental

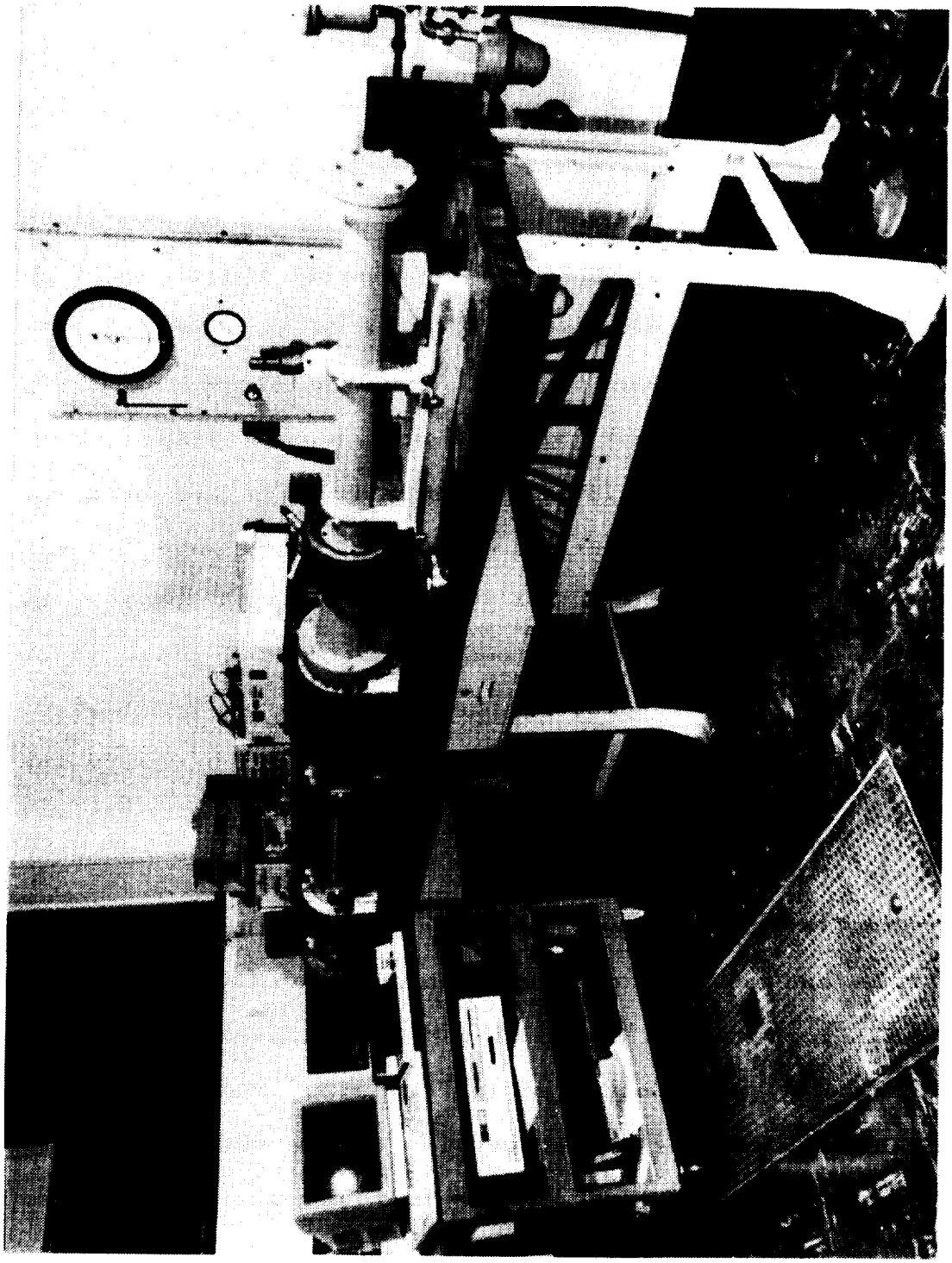

Figure 3.1. Shock Tube Assembly

information is seen schematically in Fig. 3.2. In referring to Fig. 3.2, note that the shock tube contains three sets of downstream ports on the tube wall. Two PCB 112A21 Piezotronic High-Resolution Pressure Transducers are placed in the top ports at positions 1 and 2 of the shock tube. A pressure transducer is mounted in the top port at position 2 to give an accurate measure of the speed of the shock wave as the wave travels down the shock tube. By noting the time-synched transducer responses displayed by the Gould Digital Oscilloscope, measurements are obtained for the time interval during which the shock wave travels from position 2 to position 1 of the shock tube. By knowing the distance between positions 1 and 2 (24.0 in or 61.0 cm), the actual speed of the shock wave is calculated. Consequently, this calculation gives a means to verify the predicted theoretical wave speed determined from normal shock equations [8].

The hot-film sensor is placed on an insulating foam substrate and mounted on a plug placed in the position 1 side wall port of the shock tube. The physical dimensions of the sensor are illustrated in Fig. 3.3. Judge [9] gives a listing of the material properties of the hot-film sensor and substrate. The anemometer and pressure transducer signals at position 1 of the shock tube are synchronized in time in order to show the simultaneous variation in the anemometer response and pressure transducer response. A Type T thermocouple is inserted into the top port at

ORIGINAL PAGE IS
OF POOR QUALITY

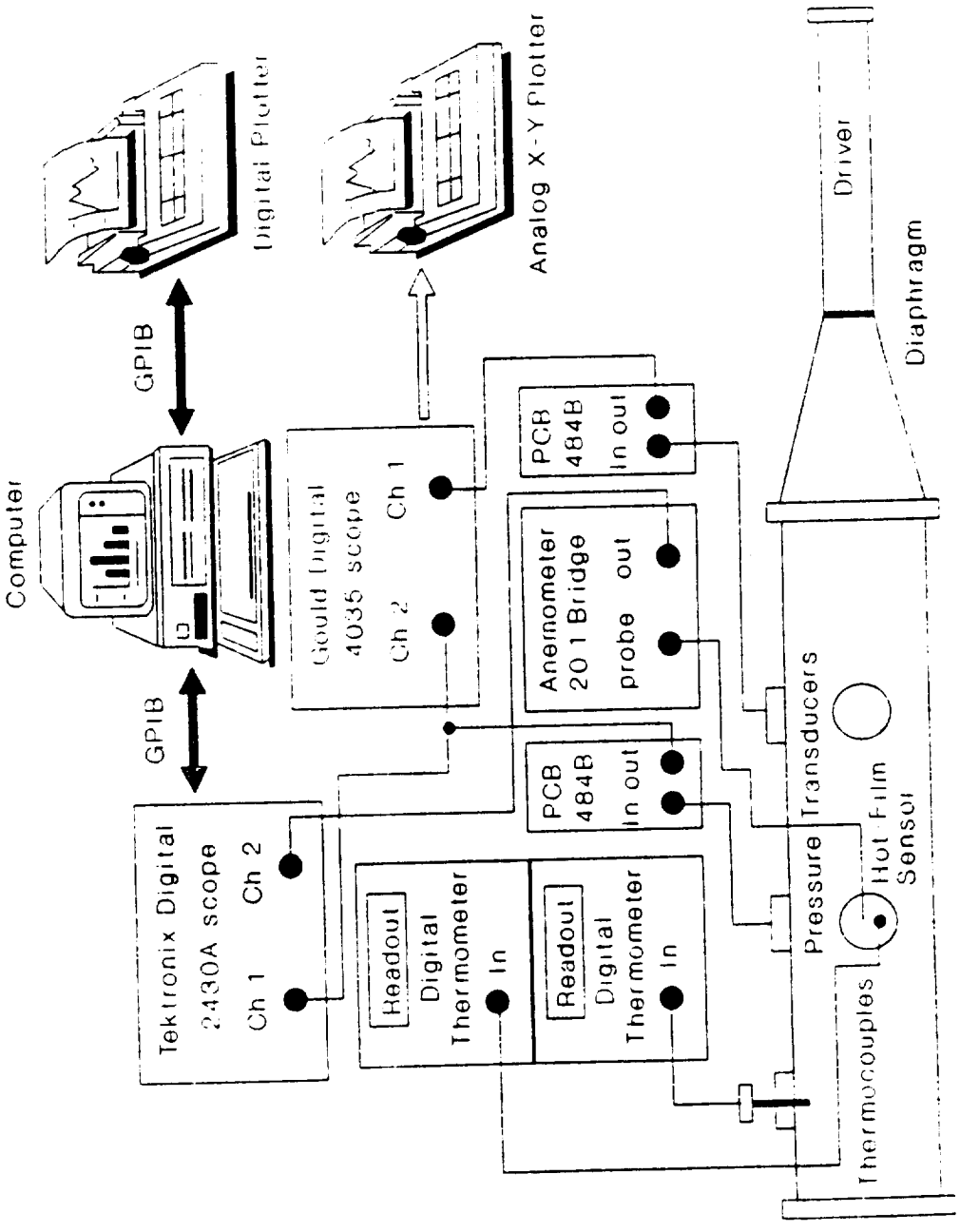

Pos. 0 Pos. 1 Pos. 2

Figure 3.2. Equipment Schematic for Shock Tube Test.

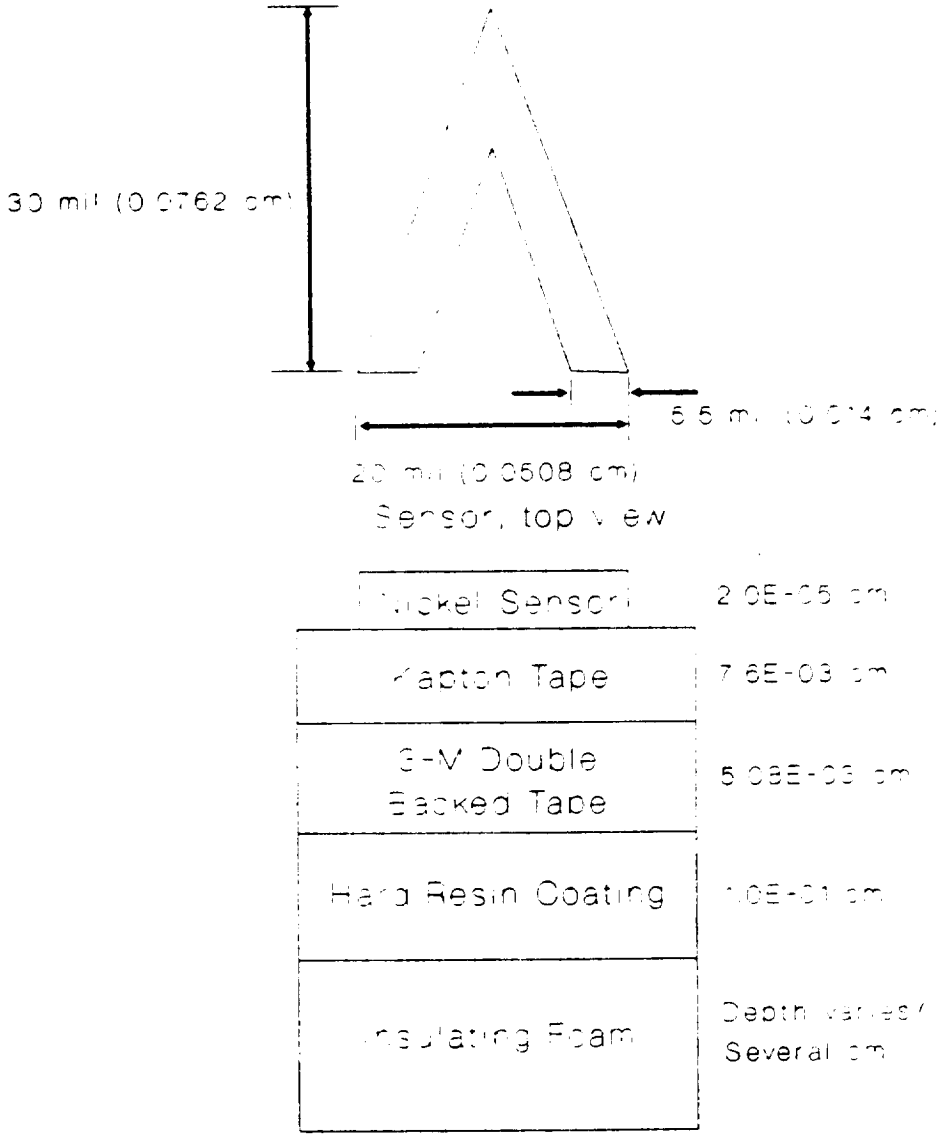

Figure 3.3 Physical Dimensions of Sensor

position 0 of the shock tube. The thermocouple extends 0.5 in (1.3 cm) from the wall into the flow and measures the ambient air temperature in the shock tube downstream of the anemometer near the endplate (Fig. 3.2). Also, a Type T thermocouple is mounted on the foam substrate beside the hot-film sensor. Figure 3.4 shows both the hot-film sensor and the thermocouple mounted on the foam substrate. The thermocouple measures the variation in the substrate temperature due to the constant elevated operating temperature at which the hot-film sensor is maintained. Initially, the hot-film sensor is maintained at an elevated temperature of 380 K which is 85 K above ambient. This corresponds to an overheat ratio of 1.3. The response of the anemometer is also tested for overheat ratios of 1.4 and 1.5 (see Section 3.3 for anemometer temperature calibrations). The overheat ratio is defined as the ratio of the heated sensor resistance to the cold sensor resistance. The effect of increasing the overheat ratio is to increase the anemometer sensitivity to mass flow fluctuations and increase the frequency response of the anemometer. The substrate temperature, measured at the thermocouple location, maintains approximately the same average temperature (22.8 ± 0.6 °C) throughout the series of tests for all three overheat ratios.

The pressure transducers are powered by two PCB 484B Line Power Units and the responses are displayed on a Gould Digital Storage Oscilloscope, Type 4035. The pressure

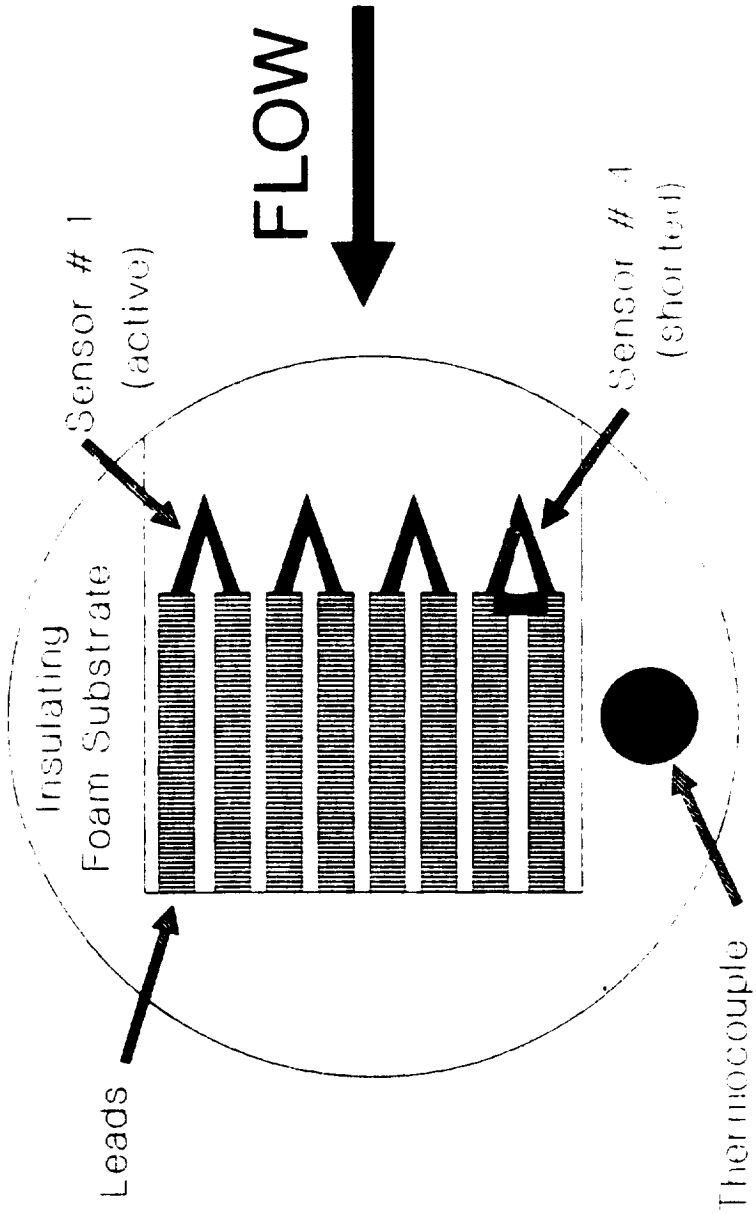

Figure 3.4. Sketch of Hot Film Sensor Plug with Thermocouple

transducer at position 1 and the anemometer are connected to channels 1 and 2, respectively of a Tektronix Digital Oscilloscope, Model 2430A. A personal computer is used as a controller for this experiment in order to initialize the Tektronix Oscilloscope parameters necessary in recording the anemometer and channel 1 pressure transducer data. A program written in GW-BASIC is used to communicate between the computer and oscilloscope via an IEEE-488 Interface. Appendix B contains a listing of the data acquisition program used in this experiment. For each test, the oscilloscope stores the voltage values of the anemometer response, which correspond to changes in the convective heat transfer across the sensor, and transfers this information onto a floppy disk for permanent record and future data analysis. The pressure transducer response at position 1 is also recorded onto a floppy disk. The pressure transducer and hot-film sensor responses recorded and displayed by each of the digital oscilloscopes are plotted for a hard copy of the output. The anemometer and channel 1 pressure transducer responses are plotted on a Hewlett-Packard 7470A Digital X-Y Plotter and both pressure transducer responses are plotted on a Hewlett-Packard 7046A X-Y Recorder. Also, a barometer is placed in the laboratory to obtain a more accurate measure of the ambient pressure at the time of testing.

3.3 Experimental Procedure

The shock tube tests are completed in a series of steps for a range of compression chamber (driver) pressures. The overheat ratio of the sensor is varied from 1.3 to 1.5 for each range of driver pressures. Also tested is the effect of the hot-film sensor response to changes in sensor orientation at the same driver pressure.

The initial set-up parameters for each test are recorded prior to the breakage of the Mylar diaphragm. These parameters are: (1) ambient temperature in the shock tube, (2) atmospheric pressure, and (3) substrate temperature. The computer adjusts the scope settings before each test and is used to record the fluctuating output voltage of the hot-film sensor due to the changes in convective heat transfer occurring across the sensor.

Before the initial testing, the anemometer's frequency response is tested using a 30 kHz square wave signal. A signal response of approximately 98 kHz is obtained with a sensor overheat ratio of 1.3. The overheat ratio of 1.3 corresponds to a total heated sensor resistance of 14.62 Ω computed by taking the sum of the shorted sensor resistance at ambient temperature multiplied by the overheat ratio plus the cable resistance. The cable resistance is frequently calibrated during the experiment and is found to be very stable. Also, the sensor reliably maintains its temperature-resistance calibration, and consequently its sensitivity and frequency response for the tests at each

particular overheat ratio. At an overheat ratio of 1.4, the total heated sensor resistance is 15.56 Ω with a frequency response of approximately 104 kHz. Also, the frequency response is approximately 105 kHz with a total heated sensor resistance of 16.56 Ω for an overheat ratio of 1.5.

The hot-film sensor is postcalibrated by WYLE Laboratories in conjunction with NASA Langley IRD. The calibration produces an indication of the temperature of the hot-film sensor at each overheat ratio. The calibration is performed by placing the sensor, mounted on the insulating foam substrate plug, into a temperature controlled air oven. The oven is elevated through a range of temperatures from approximately 15 °C to 150 °C and subsequently decreased in temperature through the same range. Using a 4-wire resistance measurement, the resistance of each sensor is recorded corresponding to the steady state temperature of the oven for each data point. The plug consists of four sensors mounted on the foam substrate (see Fig. 3.4). Sensor #4 is shorted and is used to give an indication of the lead resistance for the sensors. Only sensor #1 is used throughout the series of shock tube tests. Once the calibration is completed, a second order polynomial fit is placed through the data. Thus, an equation for the hot-film sensor calibration is obtained in which the hot-film sensor operating temperature is a function of the sensor resistance. Figure 3.5

illustrates the obtained calibration curve; and, for a specified sensor resistance at the time of testing for the corresponding overheat ratio, the operating temperature of the hot-film sensor can be obtained. The non-linear curves through the data are least squares best fits.

Before each test, the end plate of the shock tube is removed and the debris remaining inside the tube due to the diaphragm rupture is blown out. The shock tube is cleaned after each test in order to minimize the amount of flow disturbance present in the shock tube. A Mylar diaphragm is inserted into its holder and placed in position in the shock tube (see Fig. 3.2). The Mylar diaphragm is cut and shaped from a sheet of Mylar with thickness corresponding to an estimated driver rupture pressure. As the driver rupture pressure is increased, the thickness of the Mylar diaphragm is also increased. The computer program is implemented to initialize the Tektronix Oscilloscope parameters and record the anemometer and position 1 pressure transducer response data. After these procedures are completed, the driver section is pressurized until the diaphragm ruptures. At the time of the diaphragm rupture, the maximum driver pressure attained from a Wallace and Tierman pressure gauge is recorded, and the oscilloscope captures the transient anemometer and position 1 pressure transducer response data as the shock passes the hot-film sensor.

In order to capture the pressure transducer response

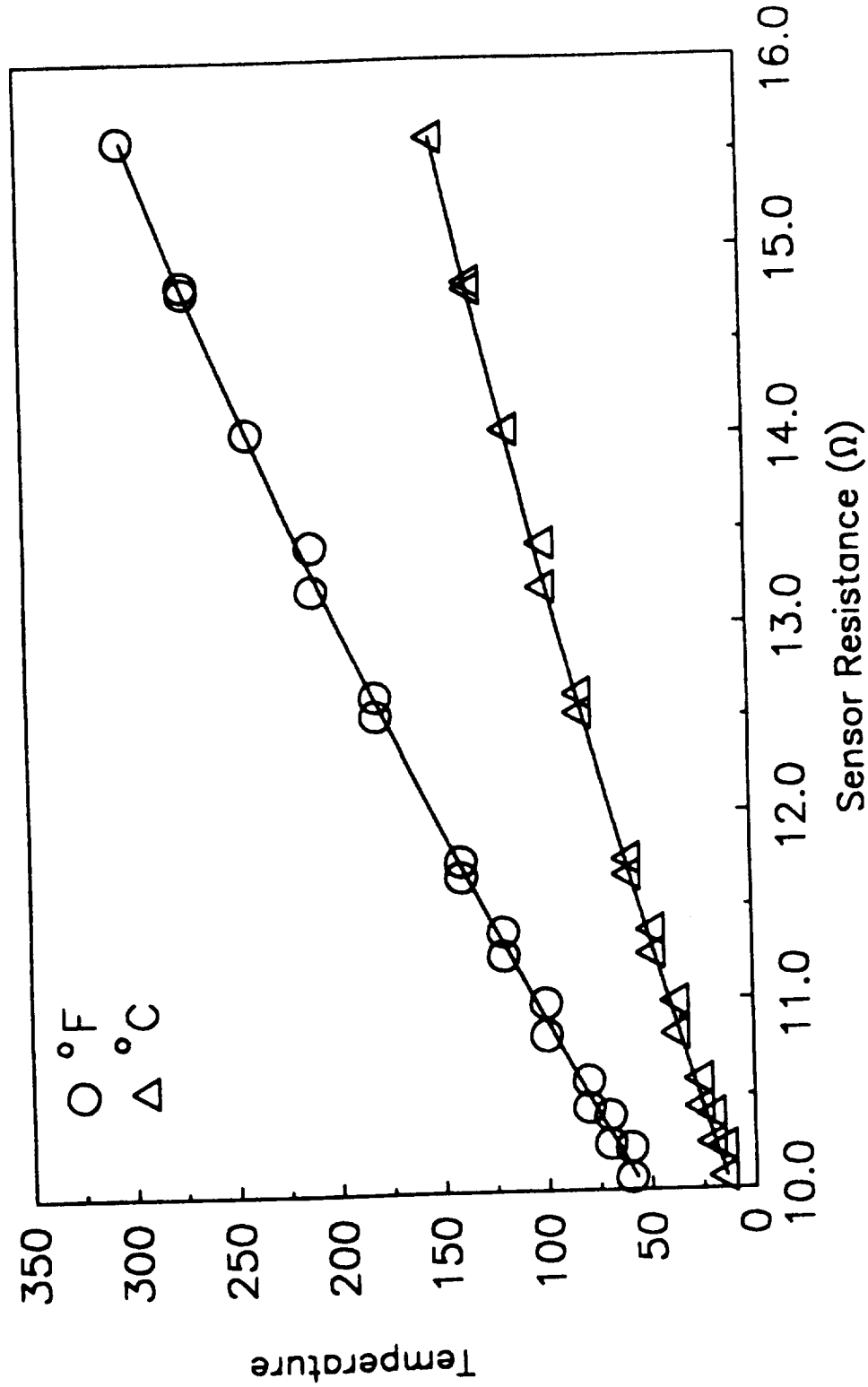

Figure 3.5. Hot–Film Sensor Calibration

and hot-film sensor response, the digital oscilloscopes are set in a pretrigger mode. The pretrigger is used to capture the initial signal of the flow disturbance prior to the passage of the shock wave. Consequently, the entire response of the anemometer and pressure transducer can be displayed and recorded by the oscilloscope. The Tektronix Oscilloscope, which captures the anemometer and position 1 pressure transducer signal, is initialized in the single sequence mode with a trigger level on channel 1 of 100 mV. As the shock passes position 1, the pressure increase due to the physical discontinuity of flow properties across the wave causes the scope to trigger. Once the 100 mV increase in voltage is obtained, which is almost instantaneously, the oscilloscope records the transient response of the pressure transducer as well as the anemometer. The Gould Oscilloscope, which records both pressure transducer responses, accomplishes the same task but the trigger level is adjusted manually to trigger off the positive rising edge of the pressure pulse.

The tests are conducted at 4 driver gauge pressures of approximately: (1) 26 psig (179 kPa), (2) 49 psig (338 kPa), (3) 56 psig (386 kPa), to (4) 79 psig (545 kPa). At each of these driver pressures, the test is repeated for which the time base of the oscilloscope is changed from 500 μs/div to 20 μs/div. The sequence of tests is performed at an overheat ratio of 1.3 and repeated for overheat ratios of 1.4 and 1.5. Once these tests are completed, the

effect of the orientation of the sensor is tested. The sensor is rotated at various angles relative to the standard operating position at a driver pressure of approximately 26 psig (179 kPa) and at an overheat ratio of 1.3 (see Fig. 3.4 for standard operating position).

3.4 Data Reduction

In order to make a comparison of the experimental results with theoretical results, the experimental data is converted into a more useful form. First note that the effects of heat conduction into the substrate are neglected since the frequency response of the substrate will not allow the substrate to respond during the approximate 3.0 ms test time. It is assumed that the hot-film sensor has been operating long enough to reach a steady-state condition. For the tests, the anemometer is switched operational approximately 15-30 minutes before the first test; long enough for the substrate heating to stabilize. The stabilization of the substrate heating is observed by monitoring the substrate thermocouple. It is also assumed that radiative heat transfer effects from the sensor are steady during the shock passage. Consequently, only the change in heat transfer from the hot-film sensor due to convection is observed during experiment times which are less than 3.0 ms.

To fully understand the development in transforming the experimental data into a more useful form, it is

necessary to understand the concept for the operation of hot-film sensors. The principle behind constant temperature anemometers is relatively simple. The electronic feedback system of the anemometer maintains the sensor temperature at a constant value. As a moving fluid convectively cools the hot-film sensor, the electronic feedback system of the anemometer increases the current supplied to the sensor in order to maintain a constant temperature. The sensor is actually one leg of a Wheatstone bridge. The sensor's electrical resistance is proportional to temperature, and the resistance becomes a measure of sensor temperature [10]. A resistance change of the sensor is compensated by the control circuit sending enough current (I_s) through the hot-film sensor to restore the bridge to its original set value. Consequently, the change in current to the sensor (I_s) determines the electrical power dissipated by the sensor, and the power increase becomes a measure of the rate of heat transfer from the sensor. Due to the assumptions of negligible changes in conduction and radiation during short experiment times, the power loss is a measure of the convective heat transfer from the hot-film sensor.

The experimental data is transformed into a more useful form by relating the output voltage of the hot-film sensor to the convective heat transfer. A series of steps is followed in order to transform the data. In order to determine the sensor current, both the mean voltage output,

measured at each overheat ratio, and the fluctuating output voltage due to the hot-film sensor reponse are used. At an overheat of 1.3, the output voltage level is measured to be 2.85 V. Also, at overheat ratios of 1.4 and 1.5, the output voltage values are measured as 3.17 V and 3.43 V, respectively. The following equation is used to determine the sensor current:

$$I_s = \frac{V_B}{50 + Rc + Rs} \tag{3.1}$$

where 50 Ω is the resistance of another leg of the Wheatstone bridge. Once the current is known, the power output of the sensor can be calculated using the following relation:

$$P_s = I_s^2 \, Rs \tag{3.2}$$

In order to negate the power supplied to the sensor due to heat losses to the substrate by conduction, a reference power level is calculated. The reference power level is calculated from the total bridge output voltage before the shock passage at time $t = 0^-$. After the shock passes across the sensor, the result is purely the power supplied to the sensor due to changes in convective heat transfer across the sensor. Equation 3.3 illustrates the resulting power equation:

$$\Delta P_{conv} = P_s - P_{ref} \tag{3.3}$$

By neglecting changes radiation heat transfer during the experimental test time and negating the effects of power loss by conduction to the substrate, the resulting power

change, ΔP_{conv}, is proportional to the convective heat transfer rate given by:

$$q = hA(T_w - T_r) \tag{3.4}$$

A best fit curve is placed through the transformed data using a computer software package. Finally, the transformed data is reduced into a nondimensional convective heat transfer parameter (i.e. Stanton number).

The laboratory frame of reference is the physical coordinate system in which the experimental data is recorded and ultimately analyzed. Consequently, the Stanton number used in the experimental analysis is derived in the coordinate system fixed with respect to the laboratory. Thus, by applying the proportionality:

$$\Delta P_{conv} \propto q_{conv} \tag{3.5}$$

and the definition of Stanton number, the resulting equation for convective heat transfer comparison becomes:

$$St = \frac{\Delta P_{conv} \nu_w}{A[T_w - T_r] k_w [u_w - u_e] \sigma_w} \tag{3.6}$$

The Reynolds number (Eq. 2.20) is derived with respect to the laboratory reference frame and can therefore be used to produce a comparison of Stanton number as a function of Reynolds number. This becomes the most useful form in comparing the experimental data to theory and experimental work produced by Davies and Bernstein [6] and Roberts, et al [13].

The following chapter contains the experimetal results. These results are transformed into nondimensional quantities for comparison with theory as well as for comparison with other experimental works [6,13]. Also obtained is a calculated heat transfer coefficient (h^*) for Judge's [9] hot-film sensor computer simulation model. The derivation of the theoretical heat transfer coefficient is discussed in detail. Finally, the shocked gas pressure ratio data is discussed in the light of the effects of the diffuser downstream of the diaphragm.

CHAPTER 4

PRESENTATION OF RESULTS

4.1 Experimental Results

The data is acquired in terms of the voltage signals for the anemometer and the pressure transducer located at position 1 of the shock tube (see Fig. 3.2). Figure 4.1 indicates the signal response of the hot-film sensor and position 1 pressure transducer at a driver pressure of 26.5 psig. As stated in Section 3.2, the pressure signals at positions 1 and 2 are recorded to determine time of flight measurements of the passing shock wave. Furthermore, by recording the pressure response at position 1, the experimentally measured pressure behind the normal shock wave can be used to deduce a shock wave speed to compare with the value found from the time of flight measurements [8]. Normal shock theory states that the pressure of the free stream gas behind the wave remains constant. From Fig. 4.1 (a), it is evident that the pressure behind the shock wave decreases at the low driver pressures in the range of 37 to 41 percent from the time the normal shock passes across the hot-film sensor to the passage of the reflected shock (a period of approximately 3 ms). This percentage increases as the driver pressure is increased.

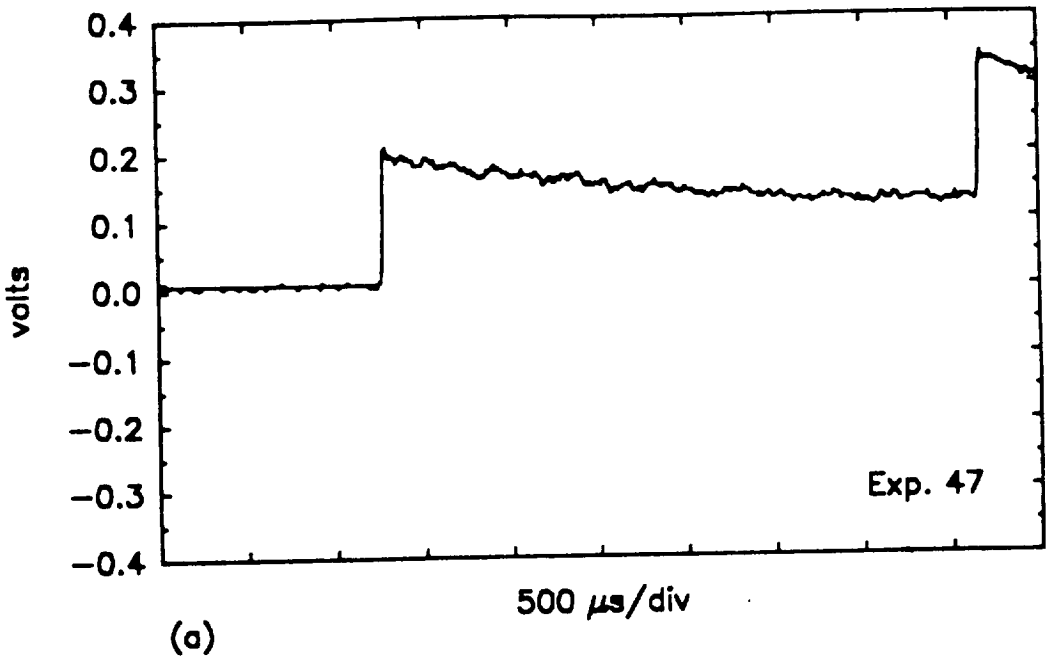

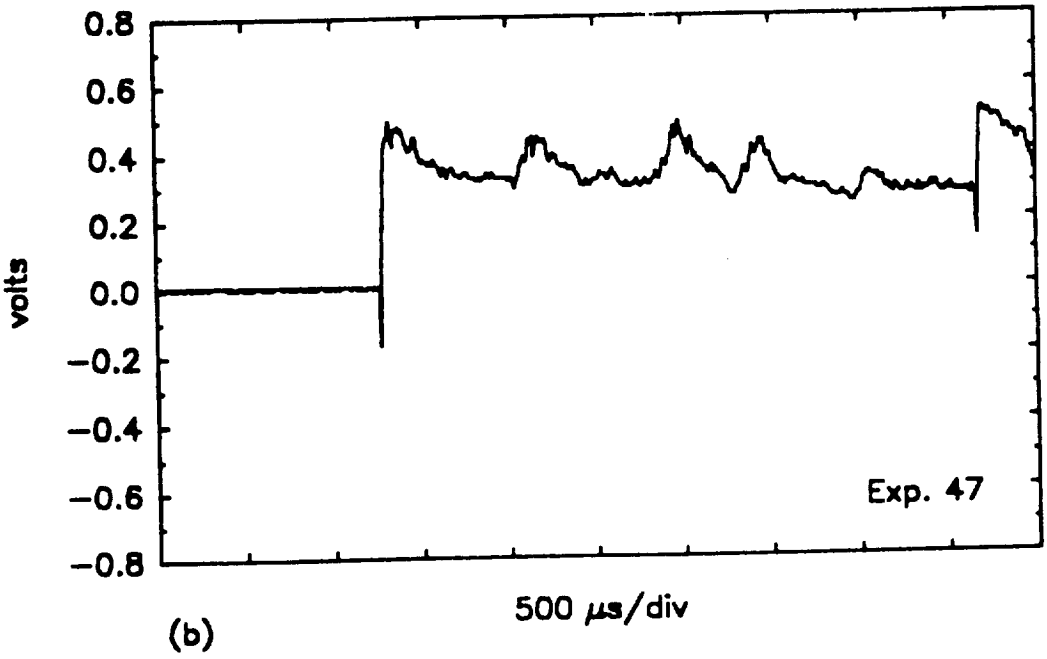

Figure 4.1. Signal Response at a Driver Pressure of 26.5 psig for the (a) Pressure Transducer, and (b) Anemometer

At the higher tested driver pressures, the decrease in pressure between the initial shock and the reflected shock varies from 47 to 51 percent. The theory used to correlate the experimental data is based on a constant free stream velocity behind the shock wave. Since the pressure response is showing a decrease from 37 to 51 percent over the test interval, this is an indication that the gas velocity is also decreasing over the test interval. The credibility of the theory is improved by identifying the experiment time interval as the first millisecond after shock passage across the hot-film sensor.

Figure 4.2 illustrates a typical anemometer response at a low driver pressure and at a higher driver pressure. The response of the hot-film sensor is nearly horizontal and is characterized by a higher frequency voltage fluctuation at the higher driver pressures (Fig. 4.2 (b)). The response of the anemometer at the lower driver pressures (Fig. 4.2 (a)) exhibits a response which quantitatively correlates with transient, compressible, turbulent boundary-layer theory over approximately the first millisecond of testing; there is otherwise little evidence of the expected power law development of a boundary layer behind the shock wave. This result seems to indicate that transition to turbulent flow is occurring very rapidly. The differences in response between the lower and higher driver pressures could be explained by less free stream turbulence occurring at the lower driver

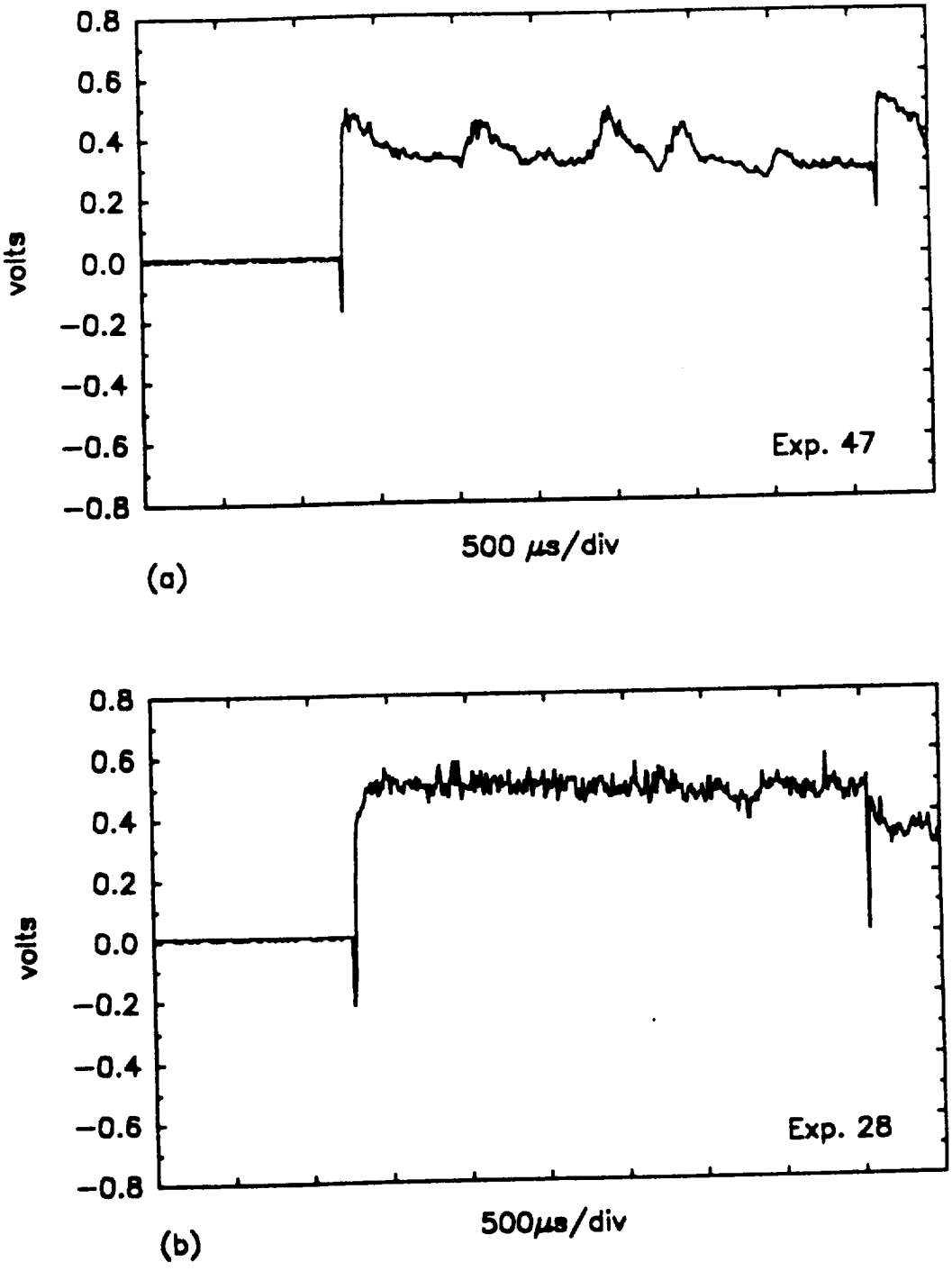

Figure 4.2. Typical Anemometer Response at Driver Pressures of (a) 26.5 psig, and (b) 78.8 psig

pressures. At the higher driver pressures, the boundary layer may be dominated by free stream turbulence which completely overcomes any ordered boundary-layer development.

Because the pressure response is decreasing over the test time, the use of the first millisecond more closely approximates a constant pressure and constant free stream velocity flow. Consequently, the correlation between experiment and theory is limited to using the lower driver pressure tests over approximately the first millisecond of anemometer response. The leading negative impulse response seen in Fig. 4.2 is discussed in Section 4.2.2.

The data set utilized for comparison with Davies and Bernstein [6] is narrowed to a set of six experimental tests. The data set consists of experiments 1-3, 22, 39, and 47. These tests were made on a 500 μs/div time base at the low range of driver pressures. The remaining tests are recorded on the smaller time base (20 μs/div) and/or at the larger driver pressures. Experiments 1-3 exhibit the same trends as the remaining three tests but are omitted from comparison with boundary-layer theory because the sensor is skewed approximately 60 degrees clockwise from the standard operating direction (see Fig. 3.4 for standard sensor orientation). This causes a gradual "roll over" of the signal response for approximately the first 0.2 ms instead of the initial peak voltage rise followed by a gradual decrease in voltage as seen in Fig. 4.2 (a). At the higher

driver pressures, the "roll over" at shock transit is more pronounced with the sensor in the 60 degree skewed orientation than at the lower driver pressures. Figure 4.3 illustrates the effect of sensor orientation for a typical set of experimental data at the mid-range of tested driver pressures. The effect of sensor orientation is further tested by rotating the sensor in 90 degree increments from the normal flow orientation and monitoring the anemometer signal response. The changes observed in sensor response due to orientation are qualitative in nature. The sensor exhibits a "roll over" in anemometer response at the initial test time as discussed previously and an initial lag in anemometer response occurs as compared to the standard sensor orientation. This lag may be attributed to the misalignment of the hot-film sensor with respect to the pressure transducer location. The shock wave passes across the pressure transducer at position 1 before passing across the hot-film sensor. This leaves a data set for comparison with Davies [6] consisting of experiments 22, 39, and 47. Figure 4.4 shows the anemometer responses obtained for each of these three experiments. Table 4.1 lists the relevant measured and calculated values of this data set. The shock velocity, u_w is determined from time of flight measurements. The measured shock velocity is within 1.0 percent of the calculated shock velocity using normal shock theory [8]. The ratio of the driven pressure to the undisturbed gas pressure (P_2/P_1) is measured using the peak

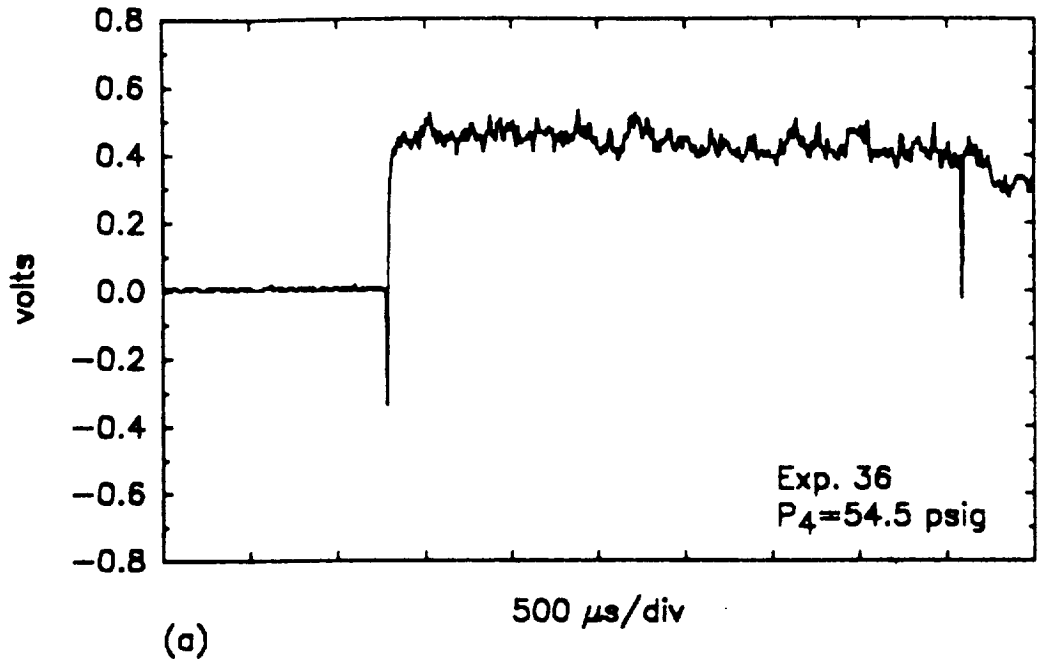

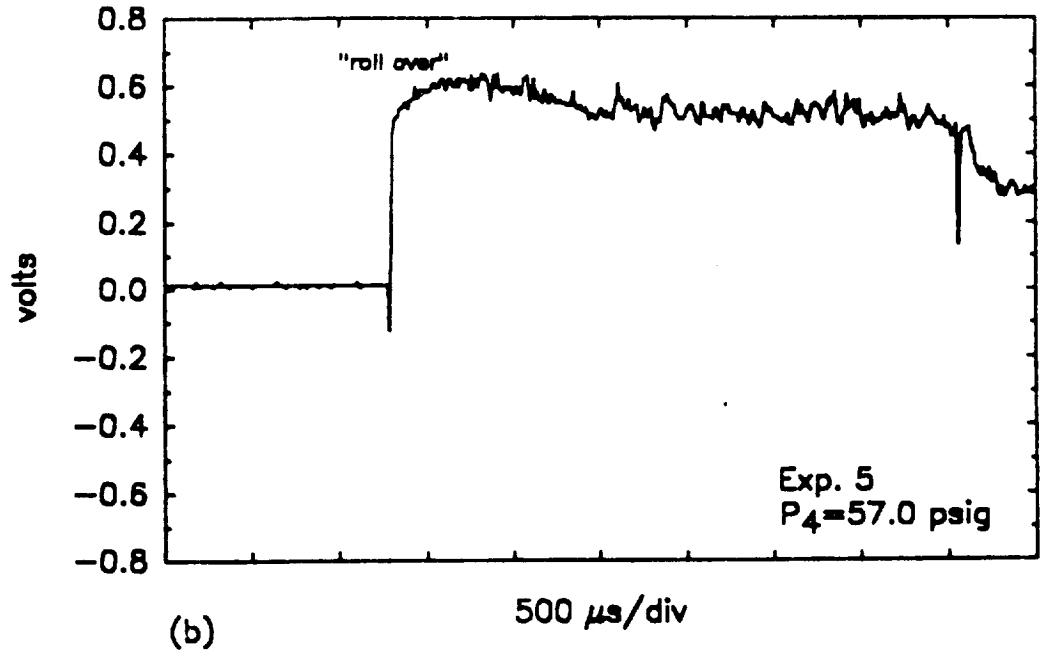

Figure 4.3. Effect of Sensor Orientation on the Anemometer Response for, (a) Normal Operating Position, and (b) 60 Degree Skewed Orientation

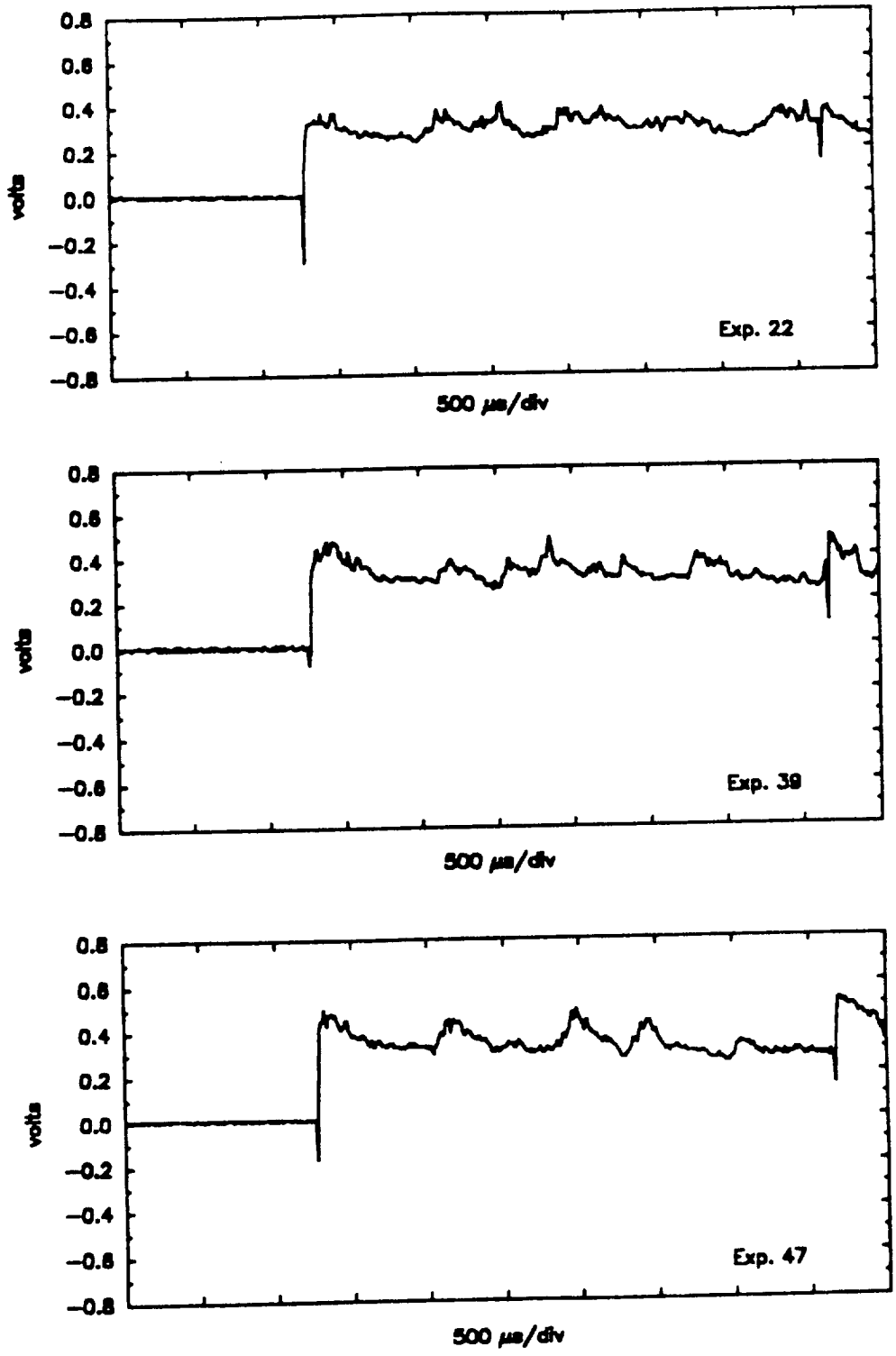

Figure 4.4. Anemometer Responses at the Lower Driver Pressures

Table 4.1. Measured and Calculated Experimental Parameters

Measured									Calculated			
Exp. No.	P4 (psig)	P1 (psia)	T_b (K)	T_{sub} (K)	T_w (K)	U_w (m/s)	P2/P1	Over Heat Ratio	U_e (m/s)	T_e (K)	T_r (K)	$h^* \cdot t^{1/5}$ $\frac{W \cdot ms^{1/5}}{m^2 K}$
22	27.0	14.9	295	296	380	385	1.29	1.3	320	318	320	220
39	26.8	15.0	295	296	400	383	1.29	1.4	321	317	319	216
47	26.5	14.9	295	296	421	383	1.28	1.5	321	317	318	214

voltage signal obtained at the time the shock passes across the sensor. The calibration factor used for the pressure transducers is 50 mv/psi. The function $h^{*} \cdot t^{\frac{1}{5}}$ is the calculated theoretical convective heat transfer coefficient for a turbulent boundary layer and will be discussed in the following section.

4.2 Heat Transfer Comparison

4.2.1. Transient Stanton Number

With the data set defined in Table 4.1, the Stanton number as a function of Reynolds number for each experiment in the data set is determined. The experimental Stanton number (Eq. 3.6) is calculated using the measured temperatures and the deduced velocities recorded at the time of the test. The remainder of the flow variables are calculated using normal shock theory. Also, the thermal and transport properties are calculated with respect to the operating temperature of the hot-film sensor since this temperature is taken to be the wall temperature (T_w). The Reynolds number is calculated using Eq. (2.20) with the further modification of Eq. (2.21) for comparison with Davies [6].

The turbulent theory for compressible, transient boundary-layer flow suggests that the Stanton number is a function of Reynolds number to the -0.2 power (see Eq. (2.30)). Consequently, by placing the data on log-log scales and taking a least squares fit of order 1, a comparison can be made between theory and experiment. The

data is placed on log-log scales and a regression of order 1 is made to obtain the coefficient and power of the best fit curve. A regression for experiment 47 is shown in Fig. 4.5. Figure 4.5 (a) shows a regression for the range of data from the time the normal shock passes across the hot-film sensor to the return of the reflected shock wave which is approximately 3.3 ms. Figure 4.5 (b) shows the regression for a segment of the data for less than the first millisecond which correlates with the turbulent boundary- layer theory. Table 4.2 lists the regression coefficients for a power law fit along with the time interval in which the regression is performed for three of the low pressure ratio experiments. Figure 4.6 shows the corresponding segment of experimental data and regression fits for the experiment numbers listed in Table 4.2.

Table 4.2. Coefficients for Power Law Curve Fit*

Exp. No.	P_4/P_1	A_0	A_1	r^2	Time (ms) from	to
22	2.82	0.317	−0.171	0.827	0.0800	0.800
39	2.79	0.402	−0.247	0.879	0.0700	0.820
47	2.78	0.279	−0.183	0.889	0.0800	0.760

*Note: $St = A_0 Re_{xs}^{A_1}$

Table 4.2 indicates a satisfactory power law curve fit over the indicated time interval. The time interval for the

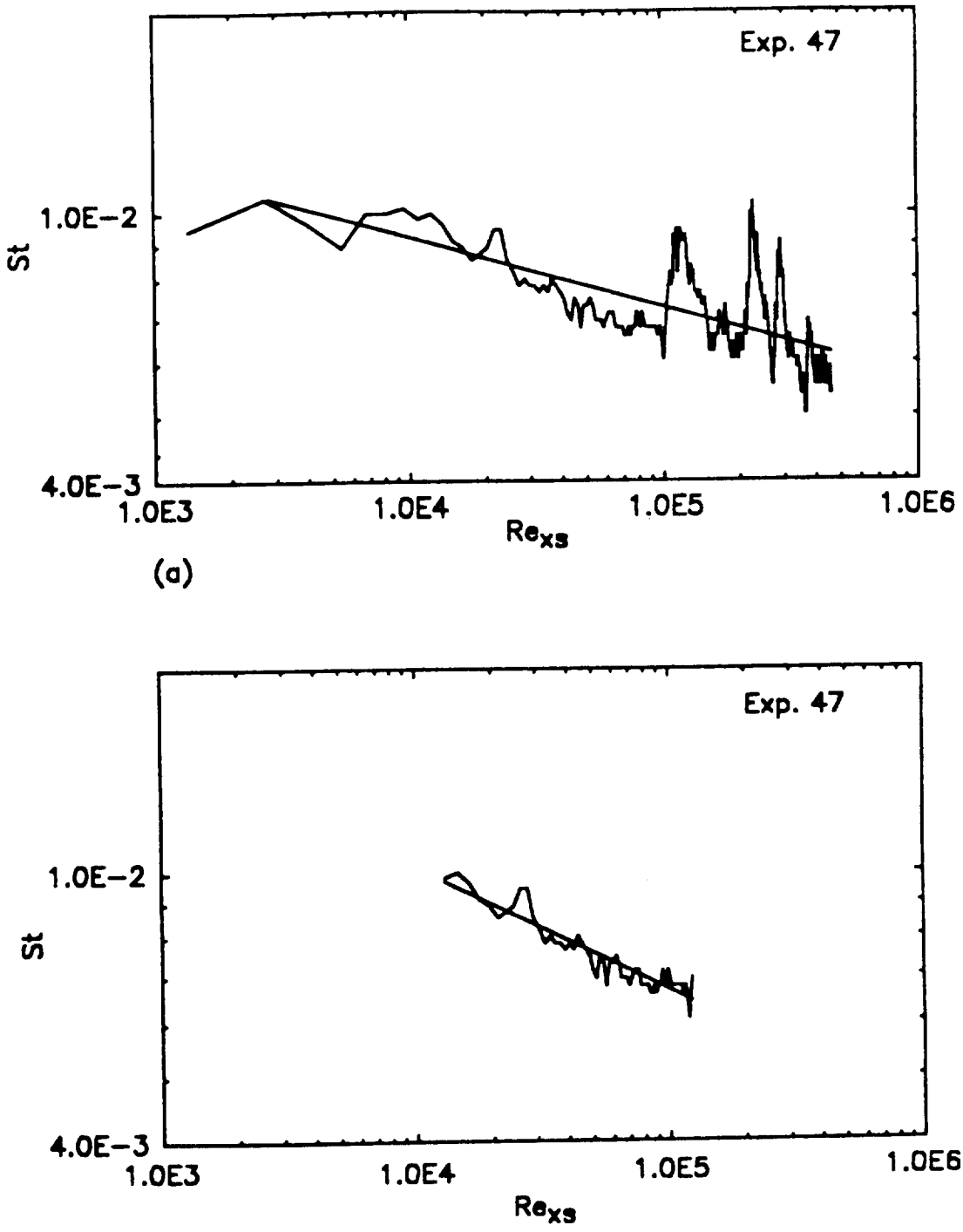

Figure 4.5. Experimental Heat Transfer Correlation at a Driver Pressure of 26.5 psig for (a) All Data within Test Time, and (b) Data within First Millisecond

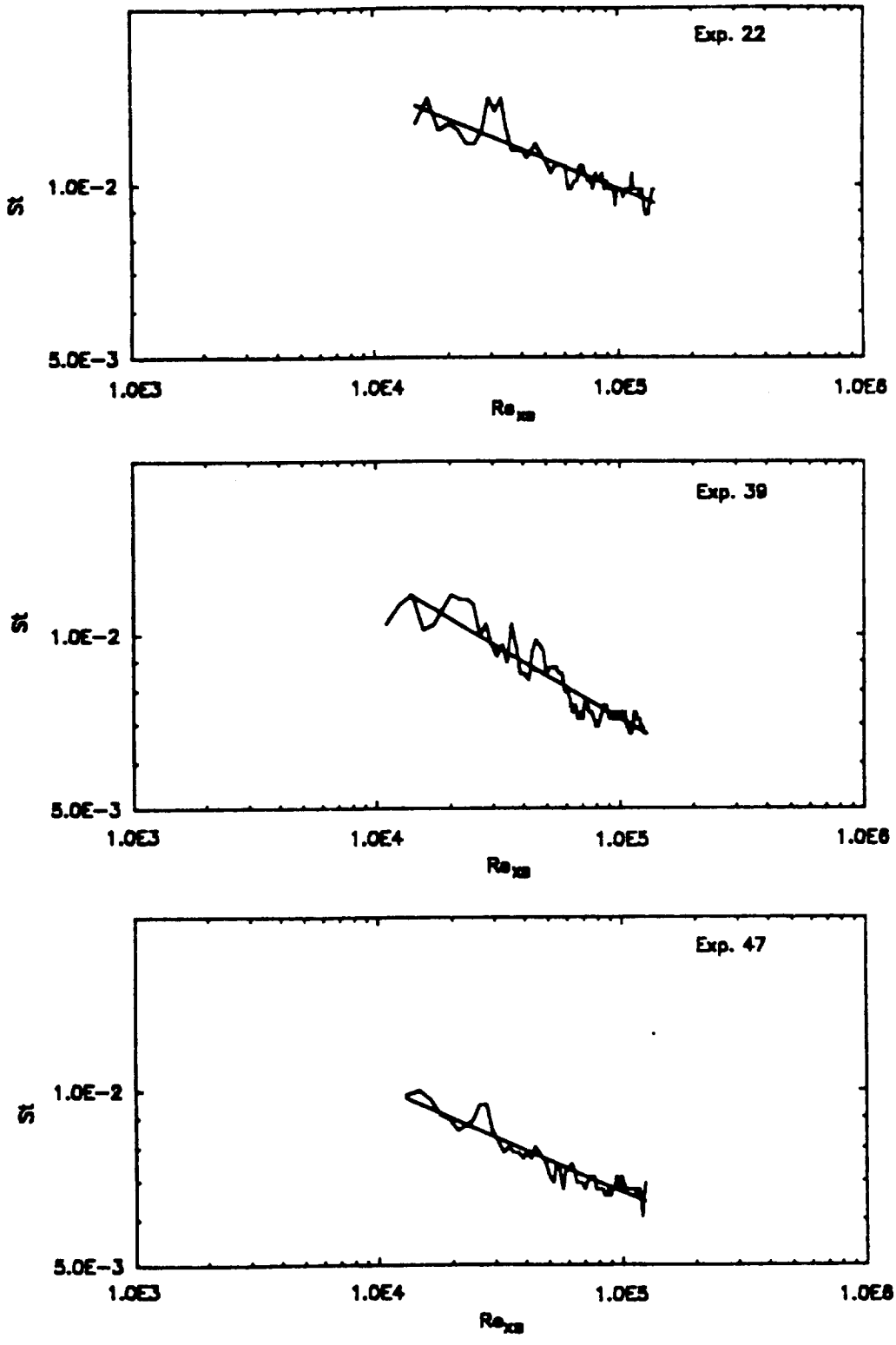

Figure 4.6. Stanton Number Power Law Regressions within the First Millisecond After Shock Transit

regression fit begins with the peak voltage value recorded by the oscilloscope until the beginning of the first large intermittent voltage fluctuation which varies from 0.760 to 0.820 ms after shock transit across the sensor. The correlation coefficent, r^2, is in the 80 percentile range, which lends evidence for the deduction that a turbulent boundary layer is developing after the shock passage.

The next step in the process of data comparison is to determine the theoretical Stanton number and compare this result with the experimental Stanton number. Using the equations developed in Section 2.4, the turbulent Stanton number as a function of Reynolds number is calculated. The theoretical transient Stanton number for experiment 47 is plotted along with the experimental Stanton number in Fig. 4.7. It is seen from Fig. 4.7 that the experimental Stanton number is higher than theory predicts for the same Reynolds number. This trend is repeated for the other two test cases, which are not shown. Plotted with the theoretical and experimental heat transfer correlations in Fig. 4.7 is the Stanton number correlation which fits Davies [6] experimental data set. The experimental work by Davies [6] also showed evidence of a laminar-to-turbulent transition, an effect not seen in the current work. Figure 4.7 gives a qualitative comparison between the work of this thesis and experimental work produced by other researchers.

A qualitative comparison is made in comparing the results of this work to the experiments conducted by

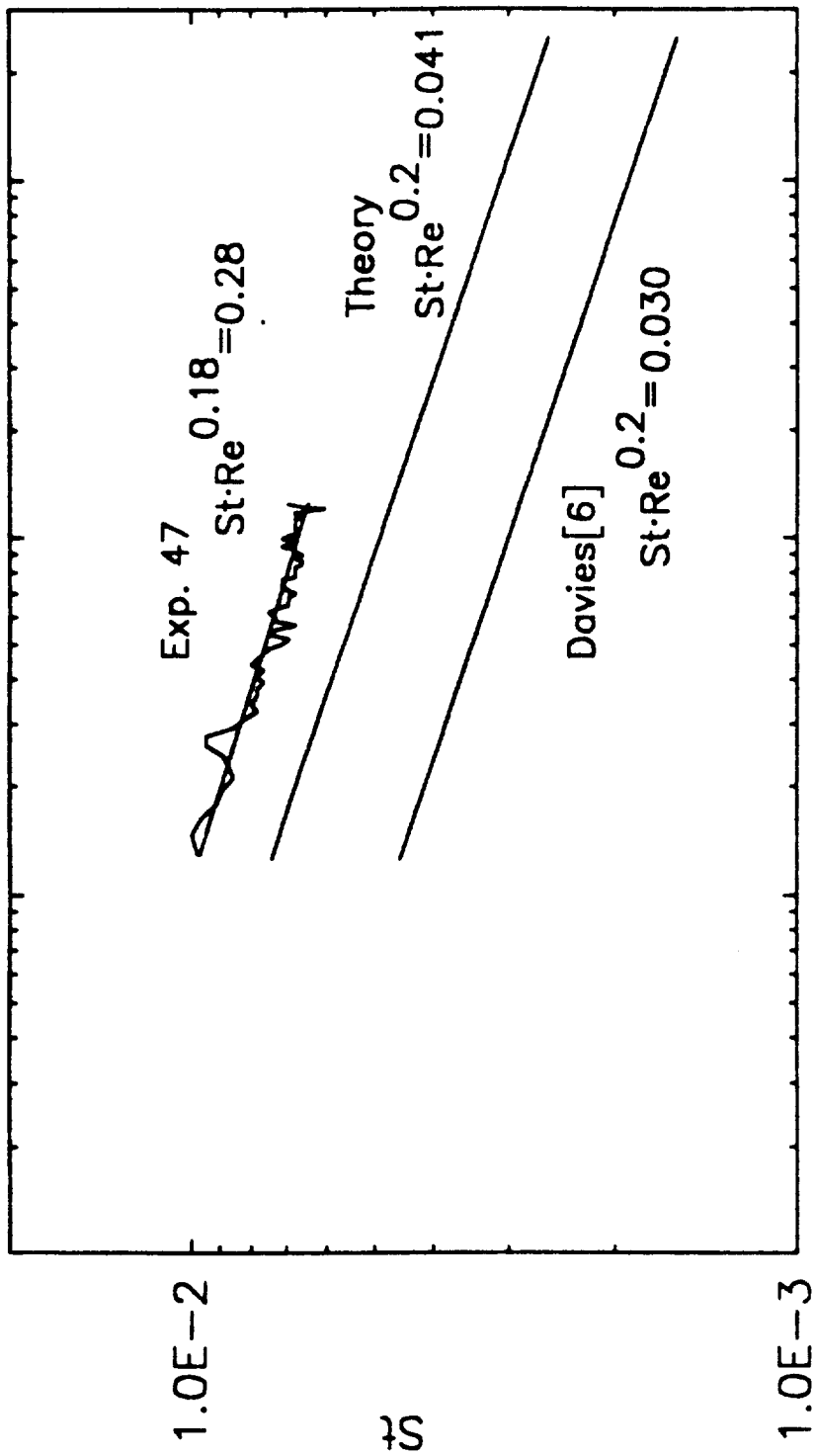

Figure 4.7. Comparison of Experimental and Theoretical Results

Roberts, et al, [13] who used very thin thermocouples mounted in the shock tube wall. Roberts, et al showed heat transfer results as a function of time for test times of 200 μs with good agreement with Mirels' turbulent boundary-layer theory [4]. The shock velocities range from 1600 to 1700 m/s which indicate that the driver pressures are much higher than those tested in this thesis. The shock velocities at the driver pressures tested in this thesis range from 382 m/s at the lowest driver pressures to 423 m/s at the highest driver pressures. The "clean" data in [13] shows the same randomness and type of fluctuations as the data obtained in this thesis. Roberts, et al [13] "dusty" data exhibits chaotic behavior over the short test period. Consequently, the conclusion may be reached that flow obstructions, such as dirt or wall roughness in the shock tube, causes the signal response of the hot-film sensor to become chaotic and prevents good agreement with transient, compressible, turbulent boundary-layer theory.

4.2.2. Heat Transfer Coefficient

A transient convective heat transfer coefficient is calculated for use as the forcing function in Judge's computer simulation of a hot-film sensor mounted on an insulating foam substrate [9]. The computer simulation can then predict the anemometer response at a given set of flow conditions. This result may serve to calibrate the hot-film sensor model. The transient heat transfer coefficient

is defined by Eq. (2.19) for a laminar boundary layer. From analyzing the experimental data in Table 4.2, it is apparent that the data correlates with turbulent boundary-layer theory. Consequently, the turbulent convective heat transfer coefficient is utilized in the computer simulation in order to compare the simulated heat flux with the experimental result. Thus, Eq. (2.32) is used to determine the theoretical heat transfer coefficient. The theoretical heat transfer coefficient used in the computer simulation requires a modification to Eq. (2.32).

The temperatures that are experimentally recorded during the shock tube tests are the ambient air temperature, T_b, and the operating temperature of the hot-film sensor, T_w. The convective heat transfer coefficient is calculated from the heat flux, where the temperature gradient is taken with respect to the recovery temperature, T_r (see Eq. (2.16)). To maintain consistency between theory, experimental data, and the computer simulation, the temperature gradient for all three is taken with respect to the free stream temperature, T_e. By adding and subtracting T_w to Eq. (2.14); and, with further algebraic manipulation, the equation for the heat transfer coefficient (Eq. (2.32)) takes the form:

$$h^* = \frac{0.0460 \cdot k_m \sigma_m^{\frac{1}{3}} (u_w - u_e)^{\frac{3}{5}}}{\nu_m^{\frac{4}{5}} t^{\frac{1}{5}}} \left[\frac{T_w \theta}{T_e \bar{\delta} \left(1 - \frac{u_w}{u_e}\right)} \right]^{\frac{1}{5}} \left[1 - \frac{r(0) Ec}{2} \right] \qquad (4.1)$$

Utilizing Eq. (4.1) as the convective heat transfer coefficient, consistency is maintained between the calculated convective heat transfer coefficient and the computer simulation model.

As noted earlier, an interesting development in the determination of the heat transfer coefficient arises in approximately the first 25 μs of the anemometer response. A very pronounced dip in anemometer response occurs in this time range as seen by viewing the experimental data in Fig. 4.8, which is recorded on a 20 microsecond time-base. The response of the hot-film sensor decreases to a negative peak voltage value and then increases sharply to a positive peak voltage value within the time frame of 25 μs. This drop in voltage increases as the driver pressure is increased. Figure 4.8 illustrates this increase in magnitude as the driver pressure is increased. Figure 3.3 shows the sensor dimensions and the value of the characteristic length (0.0762 cm). The calculated time for the shock to pass across the sensor for Exp. 38 is 2.0 μs. In the DISA paper [5], the shock front curvature was investigated by placing a hot-wire anemometer at varying distances from the shock tube wall. The results of this paper show a slight dip in the initial response of the hot-wire anemometer at a shock Mach number equal to 1.6. This is a qualitative verification that the voltage drop is characteristic of the anemometer response during passage of

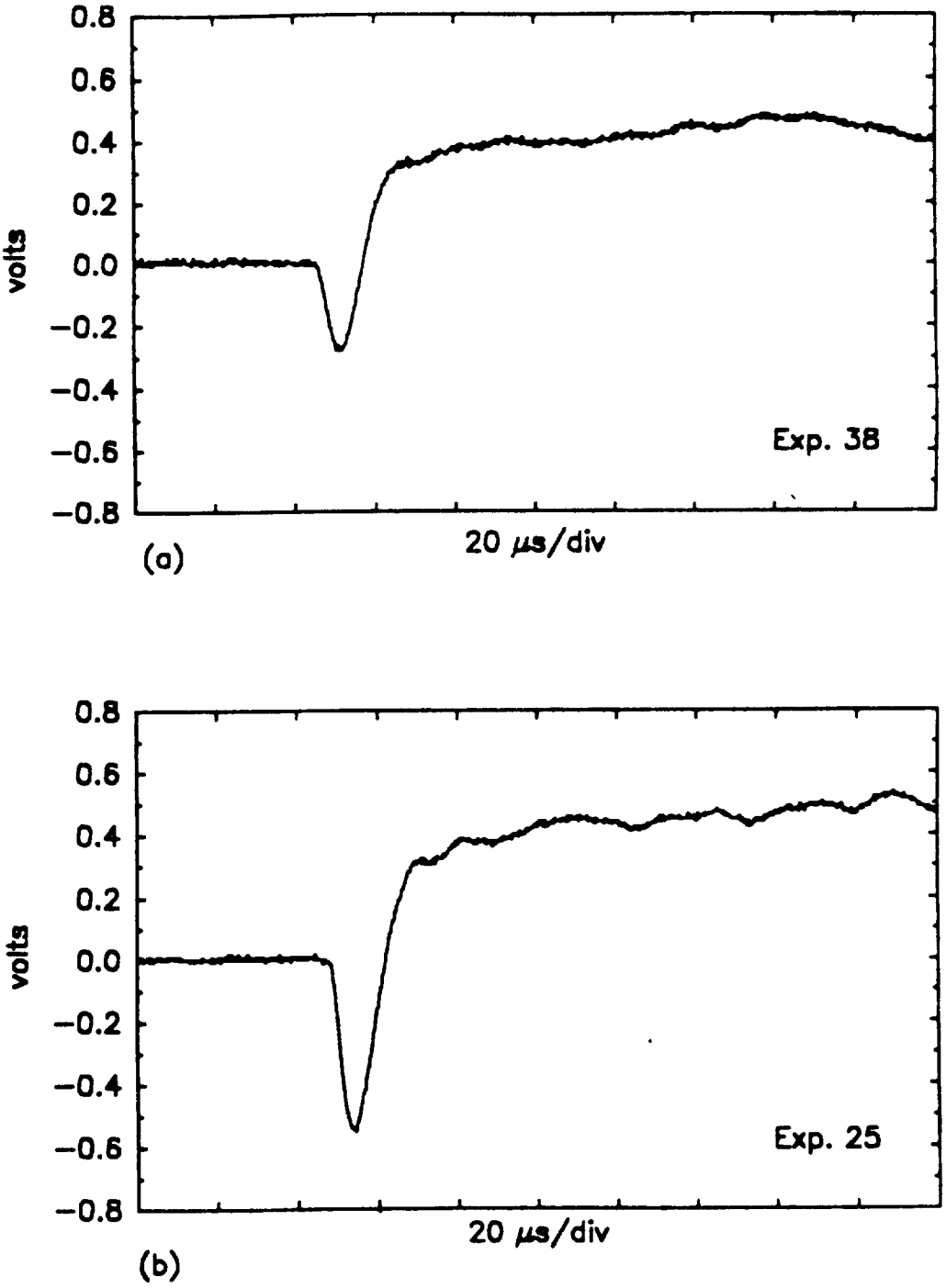

Figure 4.8. Anemometer Response Showing Wave Transit Effect, P_4= (a) 26.3 psig, and (b) 77.0 psig

a shock wave, but no works were found which clearly discuss this phenomenon.

A hypothesis is generated in order to explain the phenomenon of this drop in voltage, which corresponds to a decrease in the convective heat transfer from the hot-film sensor. It is hypothesized that as the shock passes across the hot-film sensor, the temperature of the free stream gas behind the wave rises abruptly. This assumption is based upon normal shock theory. It is further hypothesized that the step change in free stream temperature across the shock wave precedes the development of the velocity boundary layer because of a mass transport lag. Consequently, natural convective conditions prevail prior to the build-up of the shocked gas velocity boundary layer, but the sensor-gas temperature difference is less. Thus, a smaller temperature gradient along with the same natural convective heat transfer coefficient produces a sudden decrease in the heat flux from the sensor. The current supplied to the hot-film sensor to maintain its constant operating temperature is decreased, which produces the initial drop seen in the experimental results for the first few microseconds of the test. At the start of the velocity boundary-layer growth the heat flux from the sensor is a maximum since the convective heat transfer coefficient is very large. As the velocity boundary layer grows, the heat flux from the sensor decreases because of the decrease in heat escaping the boundary layer, and the anemometer

supplies less current to maintain the constant operating temperature of the hot-film sensor.

The transient convective heat transfer coefficient is divided into three parts. The first is an estimate of the amount of natural convection occurring before the start of the test from the initial power being supplied to the sensor to maintain its operating temperature. Second, a logical way of estimating the heat transfer coefficient from time t=0 to approximately t=25μs for input into the computer simulation is made based on the prior hypothesis. Finally, the transient response derived from Mirels [3] is used for times greater than measured shock transit times.

The estimate of a natural convective heat transfer coefficient is made by assuming a characteristic length equal to the area of the sensor divided by the length of the sensor (0.0762 cm). It is also assumed that this characteristic length can be associated with a small wire (horizontal cylinder). With these assumptions, Morgan [14] defines a natural convective correlation for various ranges of Grashof numbers. The Grashof number is a dimensionless parameter describing the ratio of buoyancy forces to viscous forces. After calcuating the Grashof number (approximately 0.12) and applying the correlation given by Morgan [14], an estimate of the natural convective heat transfer coefficient is made yielding a value of 8.0×10^{1} $W/m^2 \cdot K$, $\pm$ 25 percent due to the uncertainty in the correlation.

During the time that the output voltage drops and rises to its maximum value ($0<t<25\mu s$), the heat transfer coefficient is assumed to be a constant. The calculated time, using the deduced shock velocity, for the shock to pass across the sensor ranges from 1.8 to 2.0 μs at the tested driver pressures. The measured time half-way across the pressure pulse is on the order of 5 to 12 μs. A discrepency exists between the calculated shock transit time across the sensor and the measured transit time. This discrepency may be attributed in part to the lag associated with the mass transport of the gas behind the shock. Another possibility relates to the response time of the anemometer. The transit time of the shock moving across the sensor is less by a factor of 10 than the frequency response of the anemometer ($\sim$ 100 kHz). Consequently, the anemometer is not responding fast enough to capture this dip due to shock transit.

Increasing the temperature from ambient conditions to the shocked gas temperature, and evaluating the heat transfer coefficient with respect to new flow properties, does not decrease the heat transfer coefficient significantly. Thus, the convective heat transfer coefficient is maintained at its natural convective value since the decrease is assumed to be within the error of previous assumptions. The transient portion of the convective heat transfer coefficient is derived from Eq. (4.1) for a turbulent boundary layer. By combining the

three portions, a complete heat transfer coefficient is calculated for a given set of test conditions. Figure 4.9 shows a convective heat transfer coefficient curve for Exp. 47. Thus, the computer model can simulate the shock tube test cases using the combined heat transfer coefficient to predict a theoretical anemometer response. This can ultimately be compared to the experimental anemometer response.

4.3 Effects of Divergent Diffuser

It is seen from Fig. 3.2 that the NASA Langley Shock Tube has a divergent diffuser located downstream of the diaphragm. Because of the diffuser, constant area shock tube theory cannot be used to predict the pressure (P_2) behind the wave as the wave travels down the shock tube. Consequently, modifications are made in the constant area shock tube theory to account for the effects of the diffuser. Bill Chapin, working for NASA Langley IRD, developed a correction in the existing shock tube theory using steady and unsteady isentropic relations along with applying the Rankine-Hugoniot relations to account for the diffuser effect. Through a personal communication with Mr. Chapin, the correction to one-dimensional shock tube theory was obtained and used to estimate shocked gas and driver pressure ratios. Figure 4.10 shows the experimetal data for the series of shock tube tests. Also plotted is the correction in the constant area shock tube theory, which

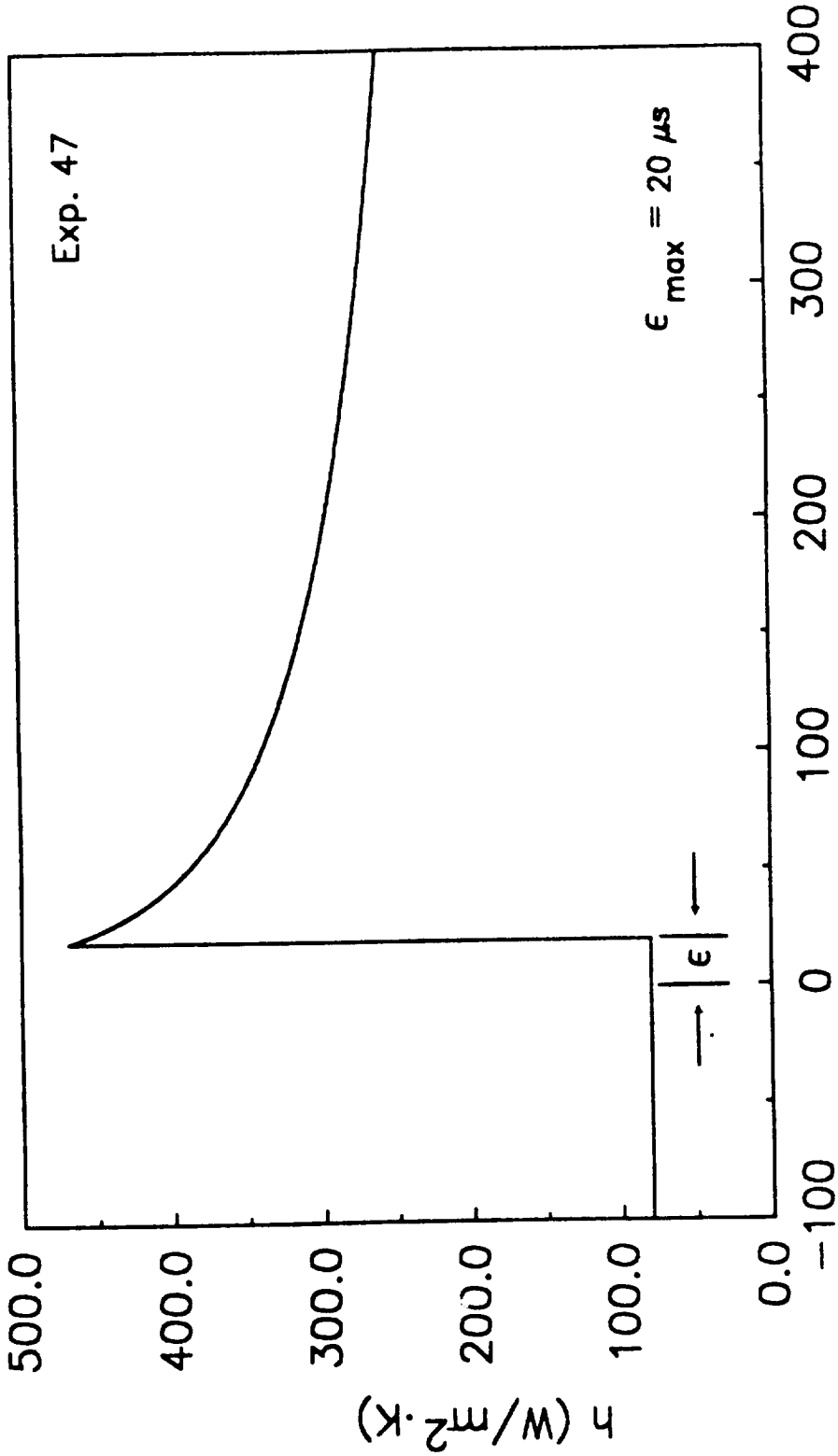

Figure 4.9. Transient Convective Heat Transfer Coefficient

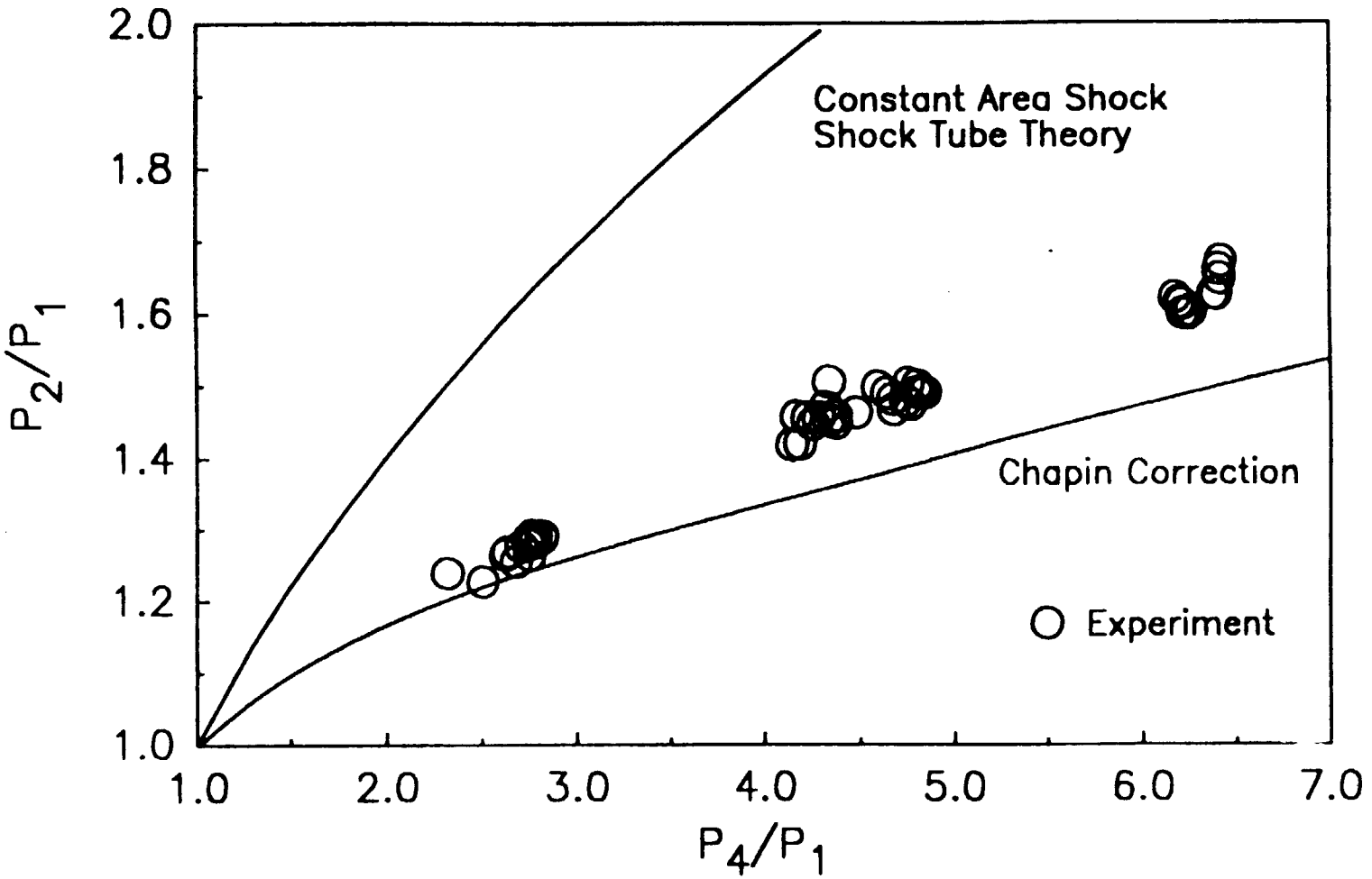

Figure 4.10. Shocked Gas Pressure Ratio Versus Driver Gas Pressure Ratio

accounts for the divergent diffuser, as well as the constant area theoretical curve. Fairly good agreement exists between the proposed correction and the test data.

The following chapter contains the conclusions drawn from the results obtained from the shock tube tests and analysis. Recommendations are made which would extend the understanding of the transient response of hot-film anemometers.

CHAPTER 5

CONCLUSIONS AND RECOMMENDATIONS

The transient response of the hot-film anemometer has been analyzed with a combination of results. First, repeatable data is easily obtained at each of the tested driver pressure ranges. The experimental comparison of the data with transient turbulent compressible boundary-layer theory seems to be valid for test times ranging from 0.2 to 0.8 ms at driver pressures of approximately 26.0 psig. Even at these driver pressures with relatively good curve fits, the predicted Stanton number for turbulent flow is less than the Stanton number obtained from the experimental data. The slopes are similar (see Fig. 4.4), but the coefficients have different values. The experimental data correlates with turbulent boundary-layer theory within the first millisecond of testing. After the first millisecond, the anemometer response becomes intermittent. This may be due to flow disturbances occurring inside the shock tube due to rough walls, micro-cavities from the ports in the walls, or unsteady turbulent free stream flow.

The comparisons with other experimental works [6,13] give reasonable qualitative comparisons. The analysis of the anemometer response at the higher driver pressures must

be left to future testing under more strictly controlled test conditions. An alternative to placing the sensor on the shock tube wall must be found in order to minimize the amount of flow disturbance present in the flow field. Mounting the hot-film sensor on a surface in the center of the shock tube [6] might produce results that better correlate with theory over a wider range of driver pressures, since this will help minimize the flow disturbance due to the walls. Also, an anemometer with a higher frequency response may produce results which better correlate with compressible, boundary-layer theory. A surprising result of this work is the occurrence of reduced heat transfer as the shock wave passes the sensor. This effect has not been clearly demonstrated in the other experimental works. Further investigation is needed to fully understand this phenomenon. Only then will a reasonable means be available to predict the magnitude of this drop in voltage.

The computer simulation of the anemometer response [9] is to be investigated in an extension of this project with hope that agreement between these experimental results and predicted anemometer response will tend to validate the hot-film sensor model.

REFERENCES

1. Wusk, M. S., Carraway, D. L., and Holmes, B. J., "An Arrayed Hot-Film Sensor For Detection of Laminar Boundary-Layer Flow Disturbance Spatial Characteristics," AIAA Paper 88-4677, AIAA/NASA/AFWAL Sensors & Measurement Technologies Conference, September 7-9, 1988, Atlanta, Georgia.

2. Chiles, H. and Johnson, B., "Development of a Temperature-Compensated Hot Film Anemometer System for Boundary-Layer Transition Detection on High-Performance Aircraft," NASA Tech Memo 83732, August 1985.

3. Mirels, Harold, "Boundary Layer Behind Shock or Thin Expansion Wave Moving into Stationary Fluid," NACA TN 3712, Washington D.C., 1956.

4. Mirels, Harold, "Laminar Boundary Layer Behind Shock Advancing into Stationary Fluid," NACA TN 3401, Washington D.C., 1955.

5. Gude, K. E. and Christoffersen, J. Aa., "The Shock Front Curvature in a Shock Tube Measured with Hot-Wire Anemometers," DISA Information, No. 6, DISA Elektronik A/S, Herlev, Denmark, February, 1968.

6. Davies, W. R. and Bernstein, L., "Heat Transfer and Transition to Turbulence in the Shock-Induced Boundary Layer on a Semi-Infinite Flat Plate," Journal of Fluid Mechanics, Vol. 36, Part 1, 1969, pp. 87-112.

7. Kayes, W. M. and Crawford, M. E., Convective Heat and Mass Transfer, 2d ed., McGraw-Hill Book Co., New York, 1980, pp. 300-301.

8. John, J., Gas Dynamics, 2d ed., Allyn and Bacon, Inc., Boston, 1984.

9. Judge, D. M., "Model of Hot-Film Sensor with Substrate Effects," Masters Thesis, Old Dominion University, Norfolk, VA., 1987.

10. Fingerson, L., and Fremouth, P., Appendix 2, IFA 100 Intelligent Flow Analyzer, Instruction Manual, TSI Incorporated.

11. Eckert, Ernst R.G., "Survey on Heat Transfer at High Speeds," Tech. Rep. 54-70, Aero. Res. Lab., Wright Air Dev. Center, Wright-Patterson Air Force Base, April, 1954.

12. Holman, J. P., Heat Transfer, McGraw-Hill Book Co., New York, 1986.

13. Roberts, G. T., Kilpin, D., Lyons, P., Sandeman, R. J., East, R. A., and Pratt, N, H., "Shock Tube Measurements of Convective Heat Transfer from a High Reynolds Number, Particle-Laden Turbulent, Non-Steady Boundary Layer," Proc. 15th Int. Symposium of Shock Waves and.Shock Tubes, California, 1985.

14. Morgan, V. T., "The Overall Convective Heat Transfer from Smooth Circular Cylinders," Advances in Heat Transfer, Vol. II, Academic Press, New York, 1975.

APPENDIX A
LIST OF EQUIPMENT

Instrument	NASA I.D.
1. P.C.B. Model 484B Line Power Unit	501702
2. P.C.B. Model 484B Line Power Unit	501703
3. Wallace and Tierman Pressure Gauge (150 psi (1034 kPa) maximum)	C44598
4. Fluke 2190A Digital Thermometer	431062
5. Fluke 2190A Digital Thermometer	427579
6. Mylar sheets for shock tube diaphragms	
7. NASA Langley Shock Tube	
8. Gould Digital Storage Oscilloscope, Type 4035	138584
9. Hewlett-Packard Digital X-Y Plotter, Model 7470A	403822
10. Hewlett-Packard X-Y Recorder, Model 7046A	532098
11. Bendix Model 790 Microbarograph	C01791
12. Two P.C.B. Piezotronic High-Resolution Pressure Transducers, Models 112A21 (sensitivity=50mv/psi)	
13. Anemometer	
a. Dantec Type 55M01 Main Unit	054789
b. Dantec Type 55M10 CTA Standard Bridge	
c. Dantec Type 55M05 Power Pack	054790
d. 5 ft. cable (connecting hot-film sensor to CTA standard bridge)	
e. Hot-film sensor mounted on an insulating foam substrate	

Instrument	Old Dominion University I.D.
14. Tektronix Digital Oscilloscope, Model 2430A	32105
15. Maxar 386 AT Computer with HP-IB Board	33157

APPENDIX B

DATA ACQUISITION PROGRAM LISTING

```
10    '  Set up program for MS-DOS HP-IB I/O Library
20    '  For use independent of the PC instrument bus system
30    DEF SEG
40    CLEAR  ,&HFE00
50    I=&HFE00
60    'PCIB.DIR$ represents the directory where the library
files are located
70   PCIB.DIR$ = ENVIRON$("PCIB")
80   I$ = PCIB.DIR$ + "\PCIBILC.BLD"
90   BLOAD I$,&HFE00
100   CALL I(PCIB.DIR$, I%, J%)
110   PCIB.SEG = I%
120   IF J%=0 THEN GOTO 170
130   PRINT "Unable to load.";
140   PRINT "    (Error #";J%;")"
150   STOP
160   '  Define entry points for setup routines
170   DEF SEG = PCIB.SEG
180   O.S      = 5
190   C.S      = 10
200   I.V      = 15
210   I.C      = 20
220   L.P      = 25
230   LD.FILE = 30
240   GET.MEM = 35
250   L.S      = 40
260   PANELS   = 45
270   '  Establish error variables and ON ERROR branching
280   DEF.ERR = 50
290   PCIB.ERR$ = STRING$(64,32)
300   PCIB.NAME$ = STRING$(16,32)
310   CALL
DEF.ERR(PCIB.ERR,PCIB.ERR$,PCIB.NAME$,PCIB.GLBERR)
320   PCIB.BASERR = 255
330   ON ERROR GOTO 600
340   J=-1
350   I$=PCIB.DIR$+"\HPIB.SYN"
360   CALL O.S(I$)
370   IF PCIB.ERR<>0 THEN ERROR PCIB.BASERR
380   '  Determine entry points for HP-IB Library routines
390   I=0
400   CALL I.V(I,IOABORT,IOCLEAR,IOCONTROL,IOENTER)
410   IF PCIB.ERR<>0 THEN ERROR PCIB.BASERR
420   CALL I.V(I,IOENTERA,IOENTERS,IOEOI,IOEOL)
```

```
430   IF PCIB.ERR<>0 THEN ERROR PCIB.BASERR
440   CALL I.V(I,IOGETTERM,IOLLOCKOUT,IOLOCAL,IOMATCH)
450   IF PCIB.ERR<>0 THEN ERROR PCIB.BASERR
460   CALL I.V(I,IOOUTPUT,IOOUTPUTA,IOOUTPUTS,IOPPOLL)
470   IF PCIB.ERR<>0 THEN ERROR PCIB.BASERR
480   CALL I.V(I,IOPPOLLC,IOPPOLLU,IOREMOTE,IORESET)
490   IF PCIB.ERR<>0 THEN ERROR PCIB.BASERR
500   CALL I.V(I,IOSEND,IOSPOLL,IOSTATUS,IOTIMEOUT)
510   IF PCIB.ERR<>0 THEN ERROR PCIB.BASERR
520   CALL I.V(I,IOTRIGGER,IODMA,J,J)
530   IF PCIB.ERR<>0 THEN ERROR PCIB.BASERR
540   CALL C.S
550   I$=PCIB.DIR$+"\HPIB.PLD"
560   CALL L.P(I$)
570   IF PCIB.ERR<>0 THEN ERROR PCIB.BASERR
580   GOTO 680
590   '  Error handling routine
600   IF ERR=PCIB.BASERR THEN GOTO 630
610   PRINT "BASIC error #";ERR;" occurred in line ";ERL
620   STOP
630   TMPERR = PCIB.ERR
640   IF TMPERR = 0 THEN TMPERR = PCIB.GLBERR
650   PRINT "PC Instrument error #";TMPERR;" detected at
line ";ERL
660   PRINT "Error: ";PCIB.ERR$
670   STOP
680   COMMON PCIB.DIR$,PCIB.SEG
690   COMMON LD.FILE,GET.MEM,PANELS,DEF.ERR
700   COMMON
PCIB.BASERR,PCIB.ERR,PCIB.ERR$,PCIB.NAME$,PCIB.GLBERR
710   COMMON
IOABORT,IOCLEAR,IOCONTROL,IOENTER,IOENTERA,IOENTERS,IOEOI,IO
EOL,IOGETTERM,IOLLOCKOUT,IOLOCAL,IOMATCH,IOOUTPUT,IOOUTPUTA,
IOOUTPUTS,IOPPOLL,IOPPOLLC,IOPPOLLU,IOREMOTE,IORESET,IOSEND,
IOSPOLL,IOSTATUS,IOTIMEOUT,IOTRIGGER,IODMA
720   FALSE     = 0
730   TRUE      = NOT FALSE
740   NOERR     = 0
750   EUNKNOWN = 100001!
760   ESEL      = 100002!
770   ERANGE    = 100003!
780   ETIME     = 100004!
790   ECTRL     = 100005!
800   EPASS     = 100006!
810   ENUM      = 100007!
820   EADDR     = 100008!
830   COMMON FALSE, TRUE, NOERR, EUNKNOWN, ESEL, ERANGE,
ETIME, ECTRL, EPASS, ENUM, EADDR
840   ' End Program Set-up
850   ' User program begins
860 INPUT "Enter the file name with path for storing data :
", RESFILE$
870   ' Open the file to download the data from scope
```

```
880 OPEN RESFILE$ FOR OUTPUT AS #1
890 INPUT "Enter the EXPERIMENT number  :  ", INFO$
900 PRINT #1, TAB(5) "Experiment #  : ", INFO$
910 PRINT "User Program For TEKTRONIX 2430A Digital
Oscilloscope "
920  ' Set the addresses for GPIB card, Scope and Plotter
930 ISC = 7  : SCOPE = 13 : PLOTTER = 5
940 CRT = ISC * 100 + SCOPE
950 PLT = ISC * 100 + PLOTTER
960  ' Initialize the variables
970 MAX.ELEMENTS = 1024 : ACTUAL.ELEMENTS = 0
980 MAX.LENGTH = 255 : ACTUAL.LENGTH = 0
990 OPTION BASE 1
1000  ' Define the Array dimensions
1010 DIM WFM(1024)
1020 DIM VOLTAGE(1050)
1030  ' Reset the GPIB card by calling IORESET command
1040 CALL IORESET(ISC)
1050 TIMEOUT = 5
1060 ' Clear the Scope and set a time for the device to
respond in secs.
1070 CALL IOCLEAR(CRT)
1080 CALL IOTIMEOUT(ISC, TIMEOUT)
1090 ENABLE = 1
1100 CALL IOEOI(ISC,ENABLE)
1110 ' Set the GPIB to remote
1120 CALL IOREMOTE(ISC)
1130 CALL IOCLEAR(ISC)
1140 'TRIGGERING COMMANDS basically for setting preset
trigger points using
1150 'the Atrigger and Btrigger positions
1160 COMM$ = "atrigger source:ch1,position:04" : LENGTH =
LEN(COMM$)
1170 CALL IOOUTPUTS(CRT,COMM$,LENGTH)
1180 COMM$ = "btrigger source:ch1,position:04" : LENGTH =
LEN(COMM$)
1190 CALL IOOUTPUTS(CRT,COMM$,LENGTH)
1200 COMM$ = "PATH OFF" : LENGTH = LEN(COMM$)
1210 CALL IOOUTPUTS(CRT,COMM$,LENGTH)
1220 'Settings of the Scope
1230 ' VERTICAL Commands set up
1240 COMM$ = "VMODE CH1:ON,CH2:ON; BWLIMIT FULL" : LENGTH =
LEN(COMM$)
1250 CALL IOOUTPUTS(CRT,COMM$,LENGTH)
1260 COMM$ = "CH1 VOLTS:100E-3,VAR:0,COUPLING:AC; CH2
VOLTS:200e-3,VAR:0,COUPLING:AC" : LENGTH = LEN(COMM$)
1270 CALL IOOUTPUTS(CRT,COMM$,LENGTH)
1280 ' HORIZONTAL Commands set up
1290 COMM$="HOR ASECDIV:20E-6,BSECDIV:20E-
6,POSITION:1.28E+2":LENGTH = LEN(COMM$)
1300 CALL IOOUTPUTS(CRT,COMM$,LENGTH)
1310 ' WAVEFORM Commands set up
1320 COMM$ = "START 1; STOP 1024; DATA ENCDG:ASCII" :
```

```
LENGTH = LEN(COMM$)
1330 CALL IOOUTPUTS(CRT,COMM$,LENGTH)
1340 ' Acquisition commands
1350 COMM$ = "RUN ACQUIRE; ACQUIRE MODE:NORMAL" : LENGTH =
LEN(COMM$)
1360 CALL IOOUTPUTS(CRT,COMM$,LENGTH)
1370 CHANL = 1
1380 'Start Acquiring the DATA from SCOPE to COMPUTER
1390 IF (CHANL = 1) THEN PRINT "Reading CHANNEL 1 "
1400 IF (CHANL = 2) THEN PRINT "Reading CHANNEL 2 "
1410 PRINT #1, "Readings of Channel Number :  "; CHANL
1420 IF CHANL = 1 THEN GOTO 1440 ELSE GOTO 1450
1430 'Read the values from channel 1 or 2 depending upon
the channel
1440 COMM$ = "DATA SOURCE:CH1" : LENGTH = LEN(COMM$) : GOTO
1460
1450 COMM$ = "DATA SOURCE:CH2" : LENGTH = LEN(COMM$)
1460 CALL IOOUTPUTS(CRT,COMM$,LENGTH)
1470 ' Start getting the data values from scope
1480 COMM$ = "CURVE?" : LENGTH = LEN(COMM$)
1490 CALL IOOUTPUTS(CRT,COMM$,LENGTH)
1500 CALL IOENTERA(CRT,WFM(1),MAX.ELEMENTS,ACTUAL.ELEMENTS)
1510 COMM$ = "WFMPRE? YOFF" : LENGTH = LEN(COMM$)
1520 CALL IOOUTPUTS(CRT,COMM$,LENGTH)
1530 CALL IOENTER(CRT, YOFF)
1540 PRINT #1, "Yoff read as    : ", YOFF
1550 COMM$ = "WFMPRE? YMULT" : LENGTH = LEN(COMM$)
1560 CALL IOOUTPUTS(CRT,COMM$,LENGTH)
1570 CALL IOENTER(CRT, YMULT)
1580 PRINT #1, "Ymult read as : ", YMULT
1590 COMM$ = "WFMPRE? XINCR" : LENGTH = LEN(COMM$)
1600 CALL IOOUTPUTS(CRT,COMM$,LENGTH)
1610 CALL IOENTER(CRT, XINCR)
1620 PRINT #1, "Xincrement is read as : ",XINCR : PRINT
#1,: PRINT #1,
1630 PRINT #1, "Point        Time            Voltage"
1640 PRINT #1, "-----------------------------------"
1650 ' Get the 1024 data points read by the scope
1660 FOR I = 1 TO 1024
1670   VOLTAGE(I) = (WFM(I) - YOFF) * YMULT
1680 PRINT #1, I TAB(12) (I-1)*XINCR TAB(26) VOLTAGE(I)
1690 NEXT I
1700 CHANL = CHANL + 1
1710 IF CHANL < 3 THEN GOTO 1380
1720 INPUT "Enter the TIME of FLIGHT from GOULD Scope : ",
TFL
1730 PRINT #1, "TIME of FLIGHT : ", TFL
1740 PRINT #1, "TEKTRONIX 2430A Scope Readings"
1750 CLOSE #1
1760 ' To plot the curves on the plotter from scope follow
the instructions
1770 PRINT "                              NOTE    "
1780 PRINT : PRINT
```

```
1790 PRINT " To PLOT the waveforms follow the instructions
: "
1800 PRINT "1. Make sure NOT to touch the DIP switches of
PLOTTER"
1810 PRINT "2. Insert a blank paper in the plotter"
1820 PRINT "3. Remove the GPIB cable from the COMPUTER"
1830 PRINT "4. Using the OUTPUT button make the SCOPE to
DEVICES Mode using the SETUP Bezel"
1840 PRINT "5. Again press the OUTPUT button and press PLOT
bezel"
1850 CALL IOOUTPUTS(CRT,COMM$,LENGTH)
1860 COMM$ = "?%" : LENGTH = LEN(COMM$)
1870 END
```

NASA
National Aeronautics and Space Administration

Report Documentation Page

1. Report No.	2. Government Accession No.	3. Recipient's Catalog No.
NASA CR-181838		

4. Title and Subtitle
Transient Hot-Film Sensor Response in a Shock Tube

5. Report Date
May 1989

6. Performing Organization Code

7. Author(s)
A. S. Roberts, Jr., K. R. Ortgies, and E. Gartenberg

8. Performing Organization Report No.

10. Work Unit No.
505-61-01

9. Performing Organization Name and Address
Old Dominion University Research Foundation
P. O. Box 6369
Norfolk, VA 23508

11. Contract or Grant No.
NAG1-735

13. Type of Report and Period Covered
Contractor Report
1988-1989

12. Sponsoring Agency Name and Address
National Aeronautics and Space Administration
Langley Research Center
Hampton, VA 23665-5225

14. Sponsoring Agency Code

15. Supplementary Notes
Langley Technical Monitor: Debra L. Carraway
Final Report

16. Abstract

Shock tube experiments have been performed to determine the response of a hot-film sensor, mounted flush on the side-wall of a shock tube, to unsteady flow behind a normal shock wave. The present experiments attempt to isolate the response of the anemometer due only to the change in convective heat transfer at the hot-film surface. The experiments, performed at low supersonic shock speeds in air, are described along with the data acquisition procedure. The change in convective heat transfer is deduced from the data and the results are compared with those from transient boundary-layer theory and another set of experimental results. Finally, a transient local heat transfer coefficient is formulated for use as the forcing function in a hot-film sensor instrument model simulation.

17. Key Words (Suggested by Author(s))	18. Distribution Statement
Hot-Film Sensor Shock Tube Transient Heat Transfer	Unclassified - Unlimited Subject Category 35

19. Security Class (of this report)	20. Security Classif. (of this page)	21. No. of pages	22. Price
Unclassified	Unclassified	83	A05